BULLETIN OF CANADIAN PETROLEUM GEOLOGY
VOL. 53, NO. 4 (DECEMBER, 2005), P. 454-472

Hydrothermal dolomitization in the Lower Ordovician Romaine Formation of the Anticosti Basin: significance for hydrocarbon exploration

D. LAVOIE *and* G. CHI[1]
Ressources Naturelles du Canada
Geological Survey of Canada
490, rue de la Couronne
Québec, QC G1K 9A9
delavoie@nrcan.gc.ca

P. BRENNAN-ALPERT
and
A. DESROCHERS
Department of Geological Sciences
University of Ottawa
Ottawa, ON K1N 6N5

R. BERTRAND
Institut National de la
Recherche Scientifique
Eau-Terre-Environnement
490, rue de la Couronne
Québec, QC G1K 9A9

ABSTRACT

This study deals with the diagenetic evolution of dolostones of the Romaine Formation, from cores and outcrops on Anticosti and Mingan islands, and reports evidence for hydrocarbon migration in secondary porosity generated by high temperature / hydrothermal alteration. Four types of calcite (grouped into early (C1) and late (C2) assemblages) and six types of dolomite (grouped into 3 different (D1, D2 and D3) assemblages) are distinguished. According to fluid-inclusion and stable C-O isotope data, the early calcite group, which consists of sedimentary micrite, replacement microspar and early pore-filling calcite records near surface diagenetic environments. Early and pervasive replacement dolomites (RD1 and RD2 in the first dolomite (D1) assemblage) were formed during early burial, and are not related to porosity generation. Later replacement dolomites (RD3 and RD4 in the second dolomite (D2) assemblage) and pore-filling dolomite cements (PD1 and PD2 in the third dolomite (D3) assemblage) as well as minor sphalerite were formed from warm, saline fluids, which were likely hydrothermal in origin. Vuggy porosity was produced through brecciation and fracturing, and through some dissolution of the D1 dolomite assemblage by these hydrothermal fluids. Intercrystalline porosity was also created during formation of the D2 dolomite assemblage. The vugs were partly occluded by late-stage pore filling dolomite and calcite cements, pyrite and barite. Bitumen droplets in vugs together with hydrocarbon inclusions recorded in C2 calcite and in contemporaneous barite indicate a hydrocarbon migration event after the porosity-generating processes.

The brecciation / leaching of a precursor dolomite host is uncommon in hydrothermal dolomite hydrocarbon fields, but is recognized in the adjacent coeval pool in Newfoundland. This type of alteration in the Ordovician carbonates with the presence of a rich hydrocarbon source rock and favourable maturation are key elements for the on-going exploration efforts in this basin.

RÉSUMÉ

Cette étude traite de l'évolution diagénétique des dolomies de la Formation de Romaine, à partir de forages et d'affleurements de terrain sur les îles d'Anticosti et de Mingan, et rapporte des évidences pour une migration d'hydrocarbures dans de la porosité secondaire générée par une altération de haute température / hydrothermale des faciès de dépôt. Quatre types de calcite (regroupés en des assemblages (C1) précoce et (C2) tardif) et six de dolomite (regroupé en trois assemblages (D1, D2 et D3) distincts) sont reconnus dans les échantillons. Sur la base des inclusions fluides et des données en isotopes stables C-O, l'assemblage de calcite précoce comprenant de la micrite sédimentaire, une calcite de remplacement et une calcite précoce de remplissage de porosité, les deux derniers enregistrant des environnements de diagenèse précoce. Des dolomites de remplacement précoce généralisé (RD1 et RD2 dans le premier assemblage (D1) de dolomite) furent formées dans le domaine d'enfouissement précoce et ne sont pas associées à une porogenèse. Des dolomites de remplacement tardif (RD3 et RD4 dans le second assemblage (D2) de dolomite) et des dolomites de colmatage de porosité (PD1 et PD2 dans le troisième assemblage (D3) de dolomite) ainsi que des quantités mineures de sphalérite furent formées par des fluides salins chauds d'origine hydrothermale probable. Une porosité importante de cavité fut produite par bréchification et fracturation et en partie à la suite de la dissolution de l'assemblage D1 par ces

[1]Current address: Department of Geology, University of Regina, Regina, SK

fluides. Une porosité intercristalline fut également générée dans l'assemblage D2. Ces porosités de cavité furent partiellement colmatées par des dolomites et calcites tardives, de la pyrite et de la barite. Des gouttelettes de bitume dans les cavités de même que des inclusions fluides à hydrocarbures trappées dans la calcite C2 et la barite contemporaine, indiquent un épisode de migration d'hydrocarbures après les processus de porogenèse.

La bréchification et la dissolution d'un précurseur dolomitique ne sont pas communes dans les réservoirs d'hydrocarbures dans les dolomies hydrothermales, mais est également noté dans un champ adjacent et contemporain à Terre-Neuve. Cette altération dans la succession ordovicienne couplée à la présence d'une riche roche-mère à hydrocarbures ainsi qu'une maturation favorable sont des éléments critiques pour les efforts actuels d'exploration dans ce bassin.

Introduction

Hydrothermal dolomite (HTD) hydrocarbon reservoirs represent one of the most important exploration targets in the Paleozoic of North America and abroad (Al-Aasm, 2003; Davies, 2004, 2005). World-class oil and gas pools are hosted in Ordovician (e.g., Albion-Scipio field; Hurley and Budros, 1990) and Devonian (e.g., Ladyfern field; Boreen and Davies, 2004) HTD in the U.S.A. and Canada. Hydrothermal dolomitization, as recently considered in Machel and Lonee (2002) refers to dolomitization by fluids characterized by higher fluid temperatures than those of the ambient burial environment.

A growing interest for HTD plays in eastern Canada followed the successful drilling of an oil-filled HTD reservoir in Lower Ordovician platform carbonates of the complexly-deformed Humber Zone of Western Newfoundland (Cooper et al., 2001). Areas of interest include the Ordovician St. Lawrence platform and Taconian-deformed Humber Zone (Eaton, 2004a, b, c). Hydrothermal alteration of limestones and hydrocarbon charge have been documented in the Lower Silurian carbonates of the Acadian Gaspé Belt in northern Gaspé peninsula (Lavoie and Morin, 2004) and northern New Brunswick (Lavoie, 2005a). Hydrothermal alteration of Lower Devonian oil and gas-producing fractured carbonates in the eastern Gaspé has also been recently described (Lavoie, 2005b).

Lower Ordovician carbonates along eastern North America, from Newfoundland to Tennessee (Mussman and Read, 1986; James et al., 1989) represent an important paleoaquifer associated with karstification, dissolution and dolomitization which hosts a number of Mississippi Valley-type (MVT) Zn-Pb deposits (Kesler, 1994). The extensively dolomitized carbonates of the St. George Group in western Newfoundland host MVT deposits (Saunders et al., 1992) as well as petroleum reservoirs (Garden Hill field; Cooper et al., 2001). The development of the giant Lower Ordovician Ellenburger-type reservoirs (>2Bboe) in southeastern U.S.A. has been long interpreted to relate to meteoric karsting associated with the continental Sauk–Tippecanoe unconformity (Loucks, 1999). High temperature dolomites have been recognized in the Lower Ordovician carbonates of the southeastern U.S.A. (Montañez, 1994) and it has been recently proposed that hydrothermal fluid migration in these carbonate successions significantly enhanced porosity / permeability and should be viewed as a critical event in the development of economic reservoirs (Loucks, 2003; Smith et al., 2005).

A number of recent core, seismic, petrographic and geochemical studies (Lavoie, 1997a, b; Brennan-Alpert, 2001; Chi and Lavoie, 2001; Lynch and Trollope, 2001) independently suggested high temperature alteration of Lower Ordovician carbonates of the St. Lawrence Platform on Anticosti and Mingan islands. The Lower Ordovician carbonates are at the base of a thick Middle Ordovician–Lower Silurian carbonate succession where few but clear indicators for more high temperature alteration are recorded in the Middle Ordovician succession (Chi et al., 2001). This paper evaluates and synthesizes the evidence for alteration and hydrocarbon charge of the carbonates of the Lower Ordovician Romaine Formation. The significance of the high temperature alteration event is a key element in the ongoing exploration efforts on Anticosti Island (Lavoie, 2004; 2005b).

History of Hydrocarbon Exploration on Anticosti Island

The first exploration cycle on Anticosti Island occurred during the late 1960s to the late 1970s. ARCO Ritchfield, Lowland Exploration and Gamache Exploration and Mining Co. and SOQUIP (Société Québecoise d'Initiatives Pétrolières) drilled eight holes over this large (8,000 km^2; Fig. 1) island with, in most cases, little if any seismic guidance. A few oil and gas shows were reported, and the cores and cuttings provided valuable material for a later detailed organic matter study (maturation, source rock and hydrocarbon generation; Bertrand, 1987, 1990, 1991; Bertrand and Héroux, 1987). These studies documented favourable conditions (within oil and gas windows and presence of a good, oil-prone source rock) for the hydrocarbon potential of the island. However, only after the announcement of the successful 1995 drilling in the Lower Ordovician carbonates of nearby western Newfoundland (Cooper et al., 2001) did a new cycle of exploration on Anticosti Island start, with the Lower Ordovician Romaine Formation as the initial exploration target (Lavoie, 1997a, b). This round of exploration, led by Shell Canada, Encal and Corridor Resources and followed by Hydro-Quebec Oil and Gas, resulted in the acquisition of about 700 km of new seismic and the drilling of seven new exploration wells. Some of these wells encountered porous reservoir units in both Lower and Middle Ordovician carbonates.

Geological and Burial History

Anticosti Island and the nearby Mingan islands and adjacent mainland (Figs. 1, 2) consist of gently southwesterly-dipping carbonate-dominated Lower Ordovician (Arenigian) to Lower Silurian (Llandoverian) facies that belong to the Central St. Lawrence Platform (Desrochers, 1985; Sanford, 1993; Long, 1997). The base of the succession consists of Lower Ordovician passive margin, eustatically-controlled subtidal to peritidal third- to fifth-order shallowing-upward cycles of the Arenigian Romaine Formation which unconformably overlies the Grenvillian metamorphic basement. The Romaine Formation consists of two long term depositional sequences; a lower sequence with distinct subdivisions extending well beyond the study area and an upper sequence with a more irregular facies architecture. The lower Romaine sequence is subdivided into three distinct facies assemblages and corresponds roughly to the Arenig series of Britain and the upper Canadian to lower Whiterockian series of North America. Similar coeval shallow-water carbonate assemblages are present 300 km east of the study area in western Newfoundland (James et al., 1989), suggesting a strong eustatic control on the development of the lower Romaine sequence. The lower facies assemblage consists of basal transgressive sandstones overlain by metre-scale peritidal shallowing-upward hemicycles (i.e., 4–5th orders) typically defined by bioturbated sandy dolostones capped by microbial-laminated dolomicrites. This facies assemblage recorded the first major transgression above the Precambrian basement in the study area and was associated with the highest stand in sea level in the Early Ordovician (Barnes, 1984). The middle assemblage comprises bioturbated, fossiliferous muddy carbonates with local development of thrombolitic complexes. A coeval assemblage extending further west into Newfoundland (i.e., Catoche Formation) indicates a vast shallow subtidal shelf of similar character throughout the area and a period of sea level rise equal to or even greater than the rate of carbonate production (James et al., 1989). The upper assemblage is composed of repetitive metre-scale peritidal shallowing-upward hemicycles (i.e., 4–5th order) of mottled, stromatolitic and ripple-laminated dolomicrites capped by microbial-laminated dolomicrites. The upper facies assemblage reflects the slowing of relative sea level rise and a major shallowing of the carbonate platform. The upper boundary of this facies assemblage is also a sequence boundary, as evidenced by the presence of abundant mudcracks, tepee structures, evaporate pseudomorphs, thick dololaminite beds and mud-chip breccias of dololaminites in the uppermost cycles.

The upper Romaine sequence (likely early Whiterock in age) abruptly overlies brecciated peritidal dololaminites consisting locally of metre-scale shallowing-upward hemicycles of peritidal carbonates overlain by bioturbated fossiliferous muddy subtidal limestones. The end of Romaine sedimentation was followed by subaerial exposure related to a major sea level lowstand recorded by the regional Sauk–Tippecanoe

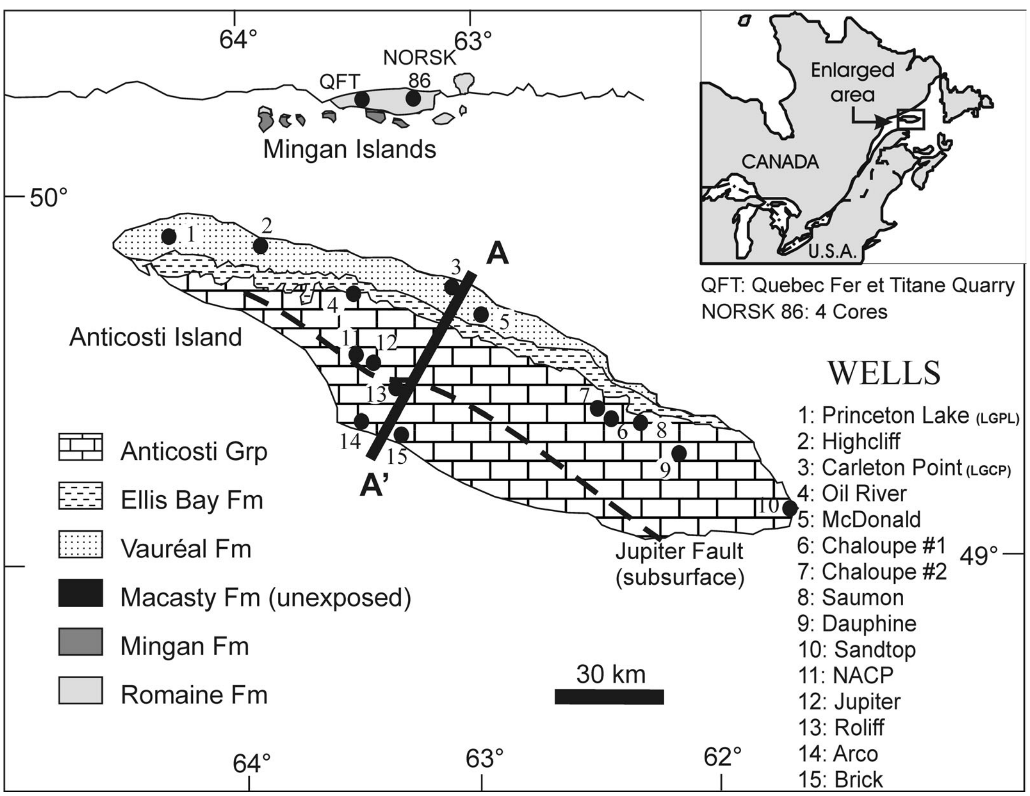

Fig. 1. General geology of Anticosti Island and the nearby Mingan Islands with the location of wells drilled on Anticosti. The Jupiter Fault is a subsurface element that does not pierce through the Silurian cover sequence. Line A–A′ locates the cross-section on Figure 2. Modified from Lavoie (1997a).

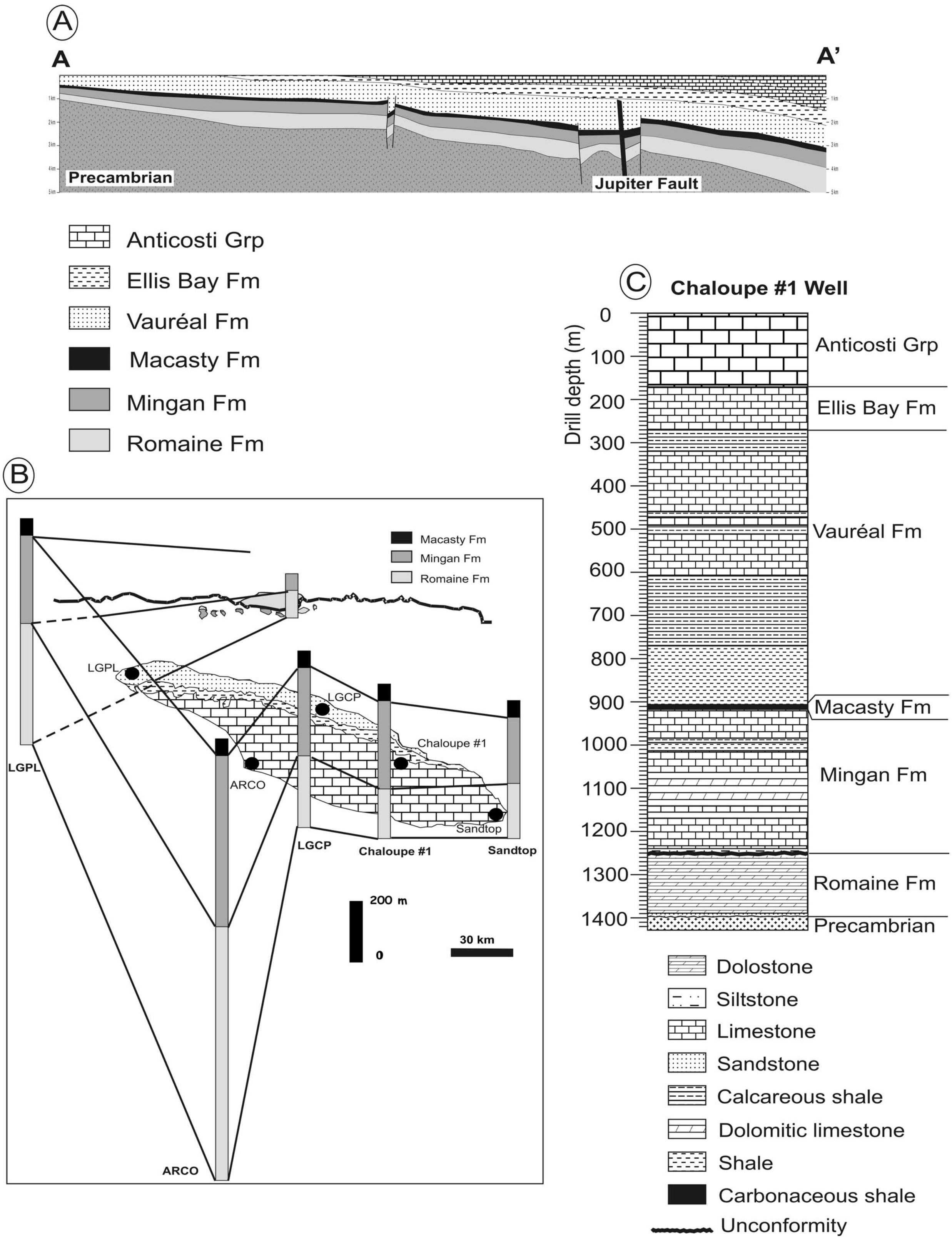

Fig. 2. **(A)** Cross-section A-A′ (see Fig. 1 for location) illustrates the gently south-dipping nature of the Anticosti platform rocks. The Jupiter Fault dies out in the Vauréal Formation (See Fig. 1 for unit symbol). Modified from Castonguay et al. (2005). **(B)** Fence diagram built from study of five wells that illustrates the thickness variations for the Romaine and Mingan formations. Thicker successions for both units occur on the southwestern side of Anticosti Island and are interpreted to be related to synsedimentary collapse of faults (including the Jupiter Fault). Modified from Lavoie (1997a). **(C)** Detailed stratigraphic section for the Ordovician–Silurian succession on Anticosti Island as recognized in the Shell et al. 2000 Chaloupe well. Dolomites are common in the Lower Ordovician Romaine Formation and occasionally occur in the Middle Ordovician Mingan Formation. Modified from Chi et al. (2001).

sequence-bounding unconformity (Desrochers, 1985; Desrochers and James, 1988). Along the continental margin of Laurentia, the development of this unconformity was enhanced by the transit of a tectonic peripheral bulge on the margin following lithospheric flexure in response to the initiation of subduction of oceanic crust (Jacobi, 1981; Knight et al., 1991). Important lateral thickness and facies changes are present within the upper Romaine sequence. The lateral facies changes are attributed to differential subsidence resulting from the onset of the foreland basin development.

The overlying succession was deposited in an active Taconian foreland setting (Lavoie, 1994). The sequence-bounding unconformity is overlain by the Middle Ordovician (Darriwilian–lower Caradocian) Mingan Formation (Desrochers, 1985) which consists of a basal transgressive sandstone unit overlain by various peritidal to open marine subtidal facies. The Mingan Formation records a tectonically-controlled sea level rise which eventually led to drowning of the carbonate ramp at the end of the Middle Ordovician. The Romaine and Mingan formations crop out on the Mingan Islands and along the adjacent mainland and were observed in all holes drilled on Anticosti Island.

The overlying units are siliciclastic-dominated. The first unit is a thin (50 m) dark marine mudstone and shale known as the Macasty Formation of Late Ordovician (late Caradocian–early Ashgillian; Riva, 1969; Achab, 1989) age. The Macasty has been shown to be a good hydrocarbon source rock (Bertrand, 1987, 1991), which, in the subsurface, has generated both oil (northern half of the island) and gas (southern half of the island) (Bertrand, 1990). This dark unit is overlain by a siltstone-dominated interval at the base of the Vauréal Formation, whereas the upper part of the Vauréal records the return of foreland carbonate sedimentation in a progressively shallower environment. The middle-late Ashgillian Vauréal Formation is the oldest outcropping unit on Anticosti Island (Riva, 1969; Achab, 1977, 1978; Copper, 1981; Fig. 1). The overlying Ellis Bay Formation is the youngest Ordovician (late Ashgillian–Hirnantian stage; Copper 1981) unit on the island. The Ellis Bay is dominated by subtidal carbonates with the local development of bioherms. The rest of the succession that crops out on the island consists of various carbonate facies with minor siliciclastics deposited on a storm-dominated carbonate ramp (Sami and Desrochers, 1992) (Fig. 2). Various formations and members are formally recognized, but for the purpose of this contribution are included within the larger Anticosti Group. The youngest unit of the Anticosti Group (the Chicotte Formation) is an uppermost Llandoverian (Telychian) unit.

The structural framework of the Anticosti island succession is straightforward (Fig. 2). From recent seismic and drill hole information, the succession can be described as a gently south-westerly-dipping homoclinal structure with no record of structural folding (Castonguay et al., 2005), although extensional faults are locally significant. The major extensional Jupiter Fault (Figs. 1, 2) is a steep NW–SE oriented plane that crosses a significant portion of the island with a downthrown southwest block. The trace of this fault is also well displayed on the regional aeromagnetic data (Oakey and Dehler, 2004). Other extensional faults have been recognized through seismic surveys (Lynch and Grist, 2002). These faults are seen affecting primarily the lower part of the succession (Romaine, Mingan, Macasty and basal Vauréal formations) and do not reach surface. Detailed core facies analysis of the Romaine Formation clearly indicates anomalous thickness variations of the unit in the southwestern segment of the island that could only be explained by local increased accommodation space associated with synsedimentary collapse of segments of the platform (Fig. 2; Lavoie, 1997a).

Based on combined organic matter reflectance and fluid inclusions data, Bertrand (1987, 1990) and Chi et al. (work in progress) proposed that burial of the Romaine Formation ranged from a maximum of 5.7 km (ARCO well, western Anticosti; Fig. 1) to a minimum of 4.4 km (LGCP well, eastern Anticosti; Fig. 1). The detailed reflectance study of Bertrand (1987, 1990) further suggested thermal gradients of 25ºC/km for the ARCO well to 26.3ºC/km and 19.7ºC/km for the LGPL and LGCP wells, respectively. With an assumed surface temperature of 25ºC, the maximum burial temperatures of the Romaine Formation would have ranged from 168ºC (ARCO well) to 112ºC (LGCP well).

Methods

From 1997 to 2001, the cored intervals of the Romaine Formation from the eight old wells on Anticosti Island and four cores on the mainland (Fig. 1) were studied in detail for facies architecture and diagenetic evolution (Lavoie, 1997a, b, 1998; Brennan-Alpert, 2001; Chi et al., 2000; Chi and Lavoie, 2001). Diagenetic study of Romaine Formation samples from a mainland quarry (QFT) north of the Mingan islands (Fig. 1) and a few samples from the Shell et al. 2000 Chaloupe well on Anticosti Island (Chi et al., 2001) was also carried out. During these studies, samples were selected from dolostone and limestone facies as well as from porous and non-porous facies, and 462 stained (Alizarin Red S-potassium ferricyanide; Dickson, 1966) conventional thin sections were examined. From this set, 67 polished thin sections were examined under cathodoluminescence (Technosyn and Nuclide luminoscopes) and 21 doubly-polished thin sections were studied for fluid inclusion microthermometry (USGS-style heating/freezing stage by Fluid Inc.). Homogenization (T_h) and final ice-melting ($T_{m\text{-}ice}$) temperatures of aqueous fluid inclusions were measured with a precision of ±1°C and ±0.2°C, respectively. API values of oils in some fluid inclusions were evaluated following the Stasiuk and Snowdon (1997) procedure.

Carbonate phases were carefully micro-drilled for oxygen and carbon stable isotope ratio analysis. One hundred and one $\delta^{18}O$ and $\delta^{13}C$ ratios were measured following standard procedures at the Geological Survey of Canada Delta Lab (42 analyses) and at the Ottawa-Carleton Derry-Rust Isotopic Lab (59 analyses). Results are expressed in the delta notation and given in permil (‰) relative to the VPDB standard. Precision of the data is better than ±0.1‰ for both $\delta^{18}O$ and $\delta^{13}C$ ratios.

Petrography

Petrographic study using transmitted light microscopy and under cathodoluminescence (CL) resulted in the recognition of early and late calcite diagenetic cementation phases and of three distinct dolomitization events in the Romaine Formation. Other significant diagenetic features (stylolites, sulphides, barite) and events (brecciation, dissolution) were also recognized.

Early calcitization event (C1 event)

Early calcitization events are generally observed in fine grained limestones mainly composed of micrite. Sedimentary micrite (SC) is iron (Fe)-poor and yellow luminescent under CL, and devoid of visible intercrystalline porosity. Replacement microspar (RC) is anhedral, 0.005 to 0.3 mm, Fe-poor, dull luminescent, and replaces micrite or fossils. An early phase of pore-filling calcite (PC1) is anhedral, 0.1 to 0.5 mm, Fe-poor, and characterized by zoned yellow/dull luminescence (Fig. 3A). These three sedimentary and diagenetic phases represent the early calcitization C1 events.

First dolomitization event (D1 event)

The earliest dolomitization event (D1) is represented by two types of petrographically similar dolomite crystals. The first replacement dolomite (RD1) is anhedral to subhedral, mainly nonplanar, very fine grained (0.005 to 0.03 mm), Fe-rich, and shows dull reddish orange luminescence. The second phase of replacement dolomite (RD2) is similar to RD1 except that it is coarser-crystalline (0.02 to 0.12 mm) and contains less Fe. RD1 and RD2 can form interstratifiated parallel laminations that display sedimentary bedding and primary facies (Fig. 3B). These two phases of dolomite are the main components of the Romaine dolostones. In general, RD1 is primarily found in peritidal depositional facies, whereas RD2 is more common in the subtidal facies assemblage. They do not possess intercrystalline porosity (Fig. 3B), but were locally subjected to later dissolution that produced pore space in the Romaine Formation carbonates (Fig. 3D).

Second dolomitization event (D2 event)

The second dolomitization event (D2) occured after some significant compaction, as indicated by local development of stylolites in RD1 and RD2 dolomite but not in dolomites of the D2 event. This event comprises two phases of dolomite replacement, designated RD3 and RD4. Phase RD3, the third phase of replacement dolomite, is anhedral to euhedral, planar to nonplanar, 0.02 to 0.5 mm in crystal size, Fe-poor with or without a Fe-rich rim, and shows dull reddish orange luminescence with or without a bright reddish orange rim. The fourth phase of replacement dolomite (RD4) is similar to dolomite RD3 except that it is uniformly Fe-rich. In most cases, these two replacement dolomite phases are associated with fractures that contribute to significant secondary porosity. In addition, both dolomites RD3 and RD4 have abundant intercrystal pore spaces (Fig. 3C) and can line inner surfaces of dissolution pores in dolomites RD1 and RD2 (Fig. 3D). The brightly luminescent rims of dolomite RD3 crystals are locally dissolved, suggesting more dissolution after the formation of dolomite RD3.

Third dolomitization event (D3 event)

Two types of vuggy pore- and fracture-filling dolomite cement (PD) are distinguished. Dolomite PD1 is subhedral to euhedral, planar to saddle, 0.1 to 0.5 mm in crystal size, Fe-poor, very dull reddish orange luminescent, and partly fills or lines vuggy dissolution pores. Dolomite PD2 is similar to dolomite PD1 except that it is Fe-rich and may have brighter reddish orange luminescent laminae (Fig. 3E). Dolomite PD2 may fill fractures and dissolution vugs. In some cores (LGCP and NACP) significant collapse brecciation forms decimetre to metre intervals of dolomitic breccia that precedes the precipitation of the void-filling dolomites. The two pore-filling dolomites (PD1 and PD2) do not coexist in the same pores or fractures, but are similar in paragenetic position, and are thus grouped as D3. Both dolomites PD1 and PD2 postdate the main secondary porosity forming event, although some corrosion and dissolution of PD1 and PD2 dolomites indicate that minor additional pore space was locally generated after or contemporaneous with D3 precipitation. In some pores of the Romaine Formation in the NACP and LGCP wells, a coating of bitumen is observed along crystal facies of D3 dolomites, which indicates an influx of hydrocarbons in the post-D3 diagenetic fluids.

Base metal precipitation

Sphalerite occurs as anhedral, coarse (1–8 mm in crystal size), yellow to brown crystals that fill fractures or vuggy pores in association with D3 dolomites (Fig. 3F). Pyrite occurs either as fine crystals (0.5–2 mm) disseminated in replacement dolomites (Py1) or as coarse crystals (2 to 10 mm) coating fractures and pores (Py2 and Py3).

Late calcite and barite precipitation

A late phase of pore-filling calcite (C2) is composed of anhedral crystals, 0.05 to 6 mm in size, that are Fe-poor to Fe-rich, fills fractures or vuggy pores still open after dolomite precipitation, and shows yellowish orange luminescence with or without patches or irregular zones of dull luminescence. Barite cement fills fractures or vuggy pores and is associated with calcite C2 phase.

Dedolomitization

In some wells on Anticosti island, partial to sometimes complete and extensive dedolomitization (calcitization of dolomite of the second dolomitization event (D2)) is observed in the northern and eastern wells of Anticosti Island (LGCP and LGPL; Lynch and Trollope, 2001; Brennan-Alpert, 2001).

Summary of paragenesis

The paragenetic sequence for the Romaine dolostone is summarized in Figure 4. The three early calcite phases (C1 event) occur mainly in limestones that have not been subject to dolomitization. The D1 dolomites appear to have been controlled by

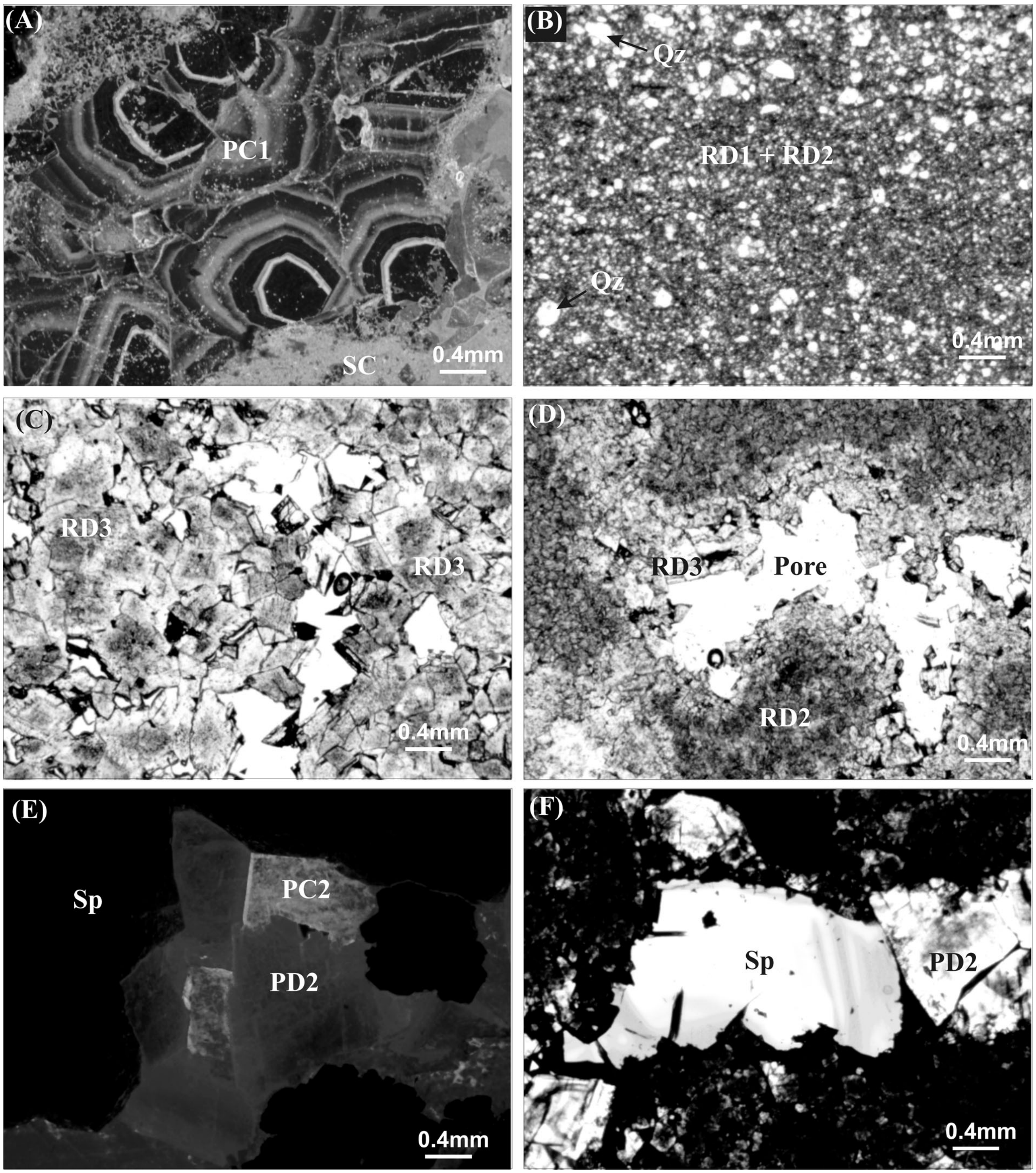

Fig. 3. Photomicrographs of the the Romaine Formation. **(A)** Cathodoluminescence light (CL) view of early pore-filling calcite (PC1) characterized by zoned yellow (pale grey) to dull (dark grey) luminescence. The cement fills a vug in a sedimentary micrite (SC). (**B)** Transmitted light view of early replacement dolomites (RD1 and RD2) which preserve bedding as indicated by the variation in grain size along horizontal bedding planes and presence of quartz grains (Qz). **(C)** Transmitted light view of RD3 dolomite showing abundant intercrystalline porosity. (**D)** Transmitted light view of vuggy porosity in RD2 dolomite. Pore walls are coated by a halo of RD3 phase dolomite crystals. **(E)** CL view of pore-filling dolomite (PD2) showing a bright reddish (grey) luminescence rim, and late pore-filling calcite (PC2) which show dull reddish orange and yellowish orange (pale grey) luminescence. Both cements precipitated over a coating of sphalerite (Sp) in a vuggy pore. **(F)** Transmitted light view of sphalerite (Sp) associated with pore-filling dolomite cement (PD2).

sedimentary textures, as indicated by their bedding-parallel distribution. They apparently postdate the early calcites but predate other minerals, and were probably formed early in the diagenetic history, before significant chemical compaction and stylolite formation. However, some RD2 dolomite may have been formed later, and overlapped in time with later dolomite phases. The D2 dolomite (RD3 and RD4) is associated with a fracture-dissolution event that created porosities in D1-rich dolostones. Later interstitial fluids were responsible locally for dedolomitization of some D2 dolomite rhombs (RD3 and RD4 dolomites). In places, RD3 dolomite shows a transitional relationship with RD2 dolomite, the main difference being that RD3 dolomite has more intercrystalline porositiy. Pyrite appears at multiple stages in the paragenetic succession, either associated with the early calcite and D1 events, or in later dissolution vugs lined by D2–D3 dolomite or later calcite (PC2). Sphalerite predates and locally partly overlaps the D3 event. The D3 dolomite (PD1 and PD2) postdates the brecciation-dissolution event, and may partly overlap with D2 in time. Bitumen coating is observed on D3 crystal faces. Calcite of the C2 event and barite are similar in paragenetic position; they both postdate the dissolution-brecciation event as well as the D3 dolomite and bitumen.

At the regional scale, dolomitization of the Romaine Formation decreases basinward (southwesterly). Peritidal facies are pervasively dolomitized (D1 to D3 events) everywhere, whereas subtidal facies are either pervasively dolomitized (Mingan Islands and onshore outcrops; D1 to D3 events) or only partly to un-dolomitized (Anticosti cores; D2 and D3 events).

Fluid Inclusion Analyses

Fluid inclusions were studied in the early calcites (C1), the D1 (RD2), D2 (RD3 and RD4) and D3 (PD1 and PD2) dolomites, and in the late calcite (C2) and barite. Fluid inclusions occurring as isolated inclusions, in clusters, or randomly

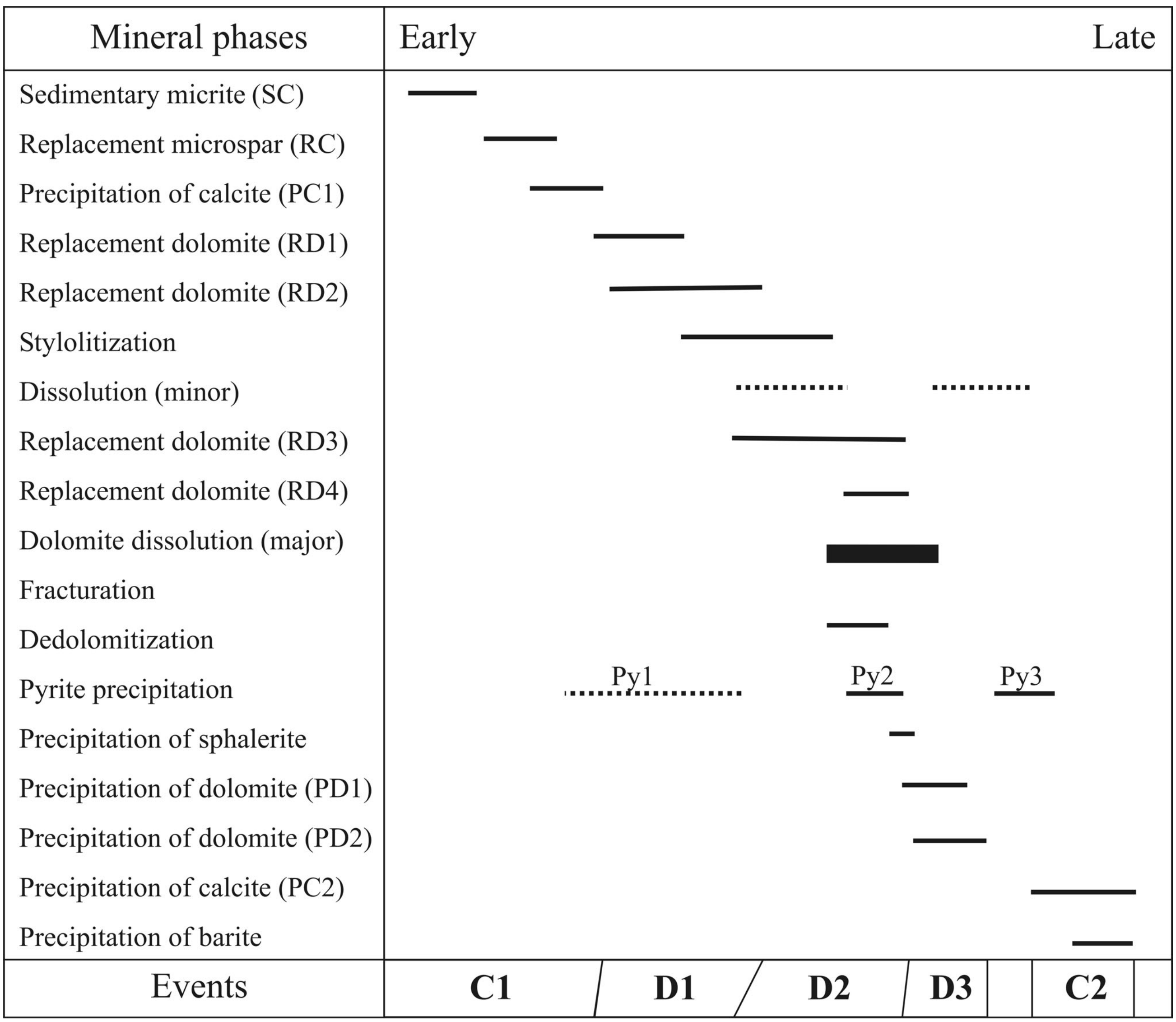

Fig. 4. Summary of the paragenetic succession in the Romaine Formation as recognized from detailed conventional and cathodoluminescence petrography. Abbreviations in text. Dotted lines represent uncertain time relationships.

distributed in three dimensions are considered as primary or pseudosecondary inclusions (Roedder, 1984). Some of the occurrences of fluid inclusions are shown in Figure 5. The microthermometric results (homogenization temperature and salinity) are listed in Table 1 and plotted in Figures 6 and 7.

Homogenization temperatures (T_h) of aqueous fluid inclusions from each mineral phase show wide ranges. However, variations within an individual inclusion group (e.g., a cluster) are much smaller, usually less than 15ºC, suggesting that post-trapping effects (e.g., stretching) are not important for most of the inclusions studied (Goldstein and Reynolds, 1994). Therefore, the overall ranges of T_h values are believed to reflect the real variation of minimum trapping temperature during the precipitation of each mineral phase (Fig. 6). Fluid inclusions from C1 calcites show very low T_h values (35 –77ºC). Fluid inclusions from RD2 (D1 event) have slightly higher T_h values, ranging from 55.6 ºC to 98.2ºC. Fluid inclusions from D2 and D3 events show higher T_h values, ranging from 59.4 ºC to 138.5°C (RD3), 78.3 ºC to 121.5° C (RD4), 60.3 ºC to 113.3°C (PD1), and 92.1 ºC to 151.2ºC (PD2). T_h values of fluid inclusions from calcite C2 and barite range from 33.8 ºC to 120.8°C and 51.5 ºC to 110.6ºC, respectively.

All aqueous inclusions (Table 1) are characterized by first-melting temperatures between –70 ºC and –50°C, and the composition of the fluids is approximated by an H_2O-NaCl-$CaCl_2$ ($MgCl_2$) system (Roedder, 1984). The final ice-melting temperatures range from –11 ºC to –47°C, corresponding to salinity values from 17 to 31 wt.% NaCl equivalent (Fig. 6).

Hydrocarbon inclusions were observed in a few samples of calcite C2 and barite. They are mainly colourless under transmitted light (Fig. 5C), fluoresce greenish white under blue light excitation, and always homogenize to a liquid phase. The L_{max} and Q values of the fluorescence spectra of oil inclusions are 510 nm and 0.044 (calcite) and 510 nm and 0.040 (barite). The API values of the oil inclusions, calculated based on the L_{max} and Q values (Stasiuk and Snowdon, 1997) are 41.1 (calcite) and 41.2 (barite). The average homogenization temperatures of the hydrocarbon inclusions are 80ºC and 59 ºC for calcite and barite, respectively, and those of aqueous inclusions are 90ºC and 81ºC for calcite and barite, respectively. If the oil and aqueous inclusions were entrapped at the same time from an oil-water immiscible fluid system, it may be assumed that the aqueous phase was saturated with hydrocarbons and that the homogenization temperature of the aqueous inclusions approximates the trapping temperature. Using the isochores of the oil inclusions constructed with the above API values and the VTFLINC program, the fluid pressures are estimated to be 345 to 392 bars (Chi et al., 2000).

Interpretation

There is an increase of homogenization temperatures of aqueous fluid inclusions from the early dolomite RD2 (average 75°C) to the dolomite PD2 (average 120°C) (Fig. 7). The T_h values of various dolomitic phases do not correlate with the geographical location of the wells and the estimated maximum

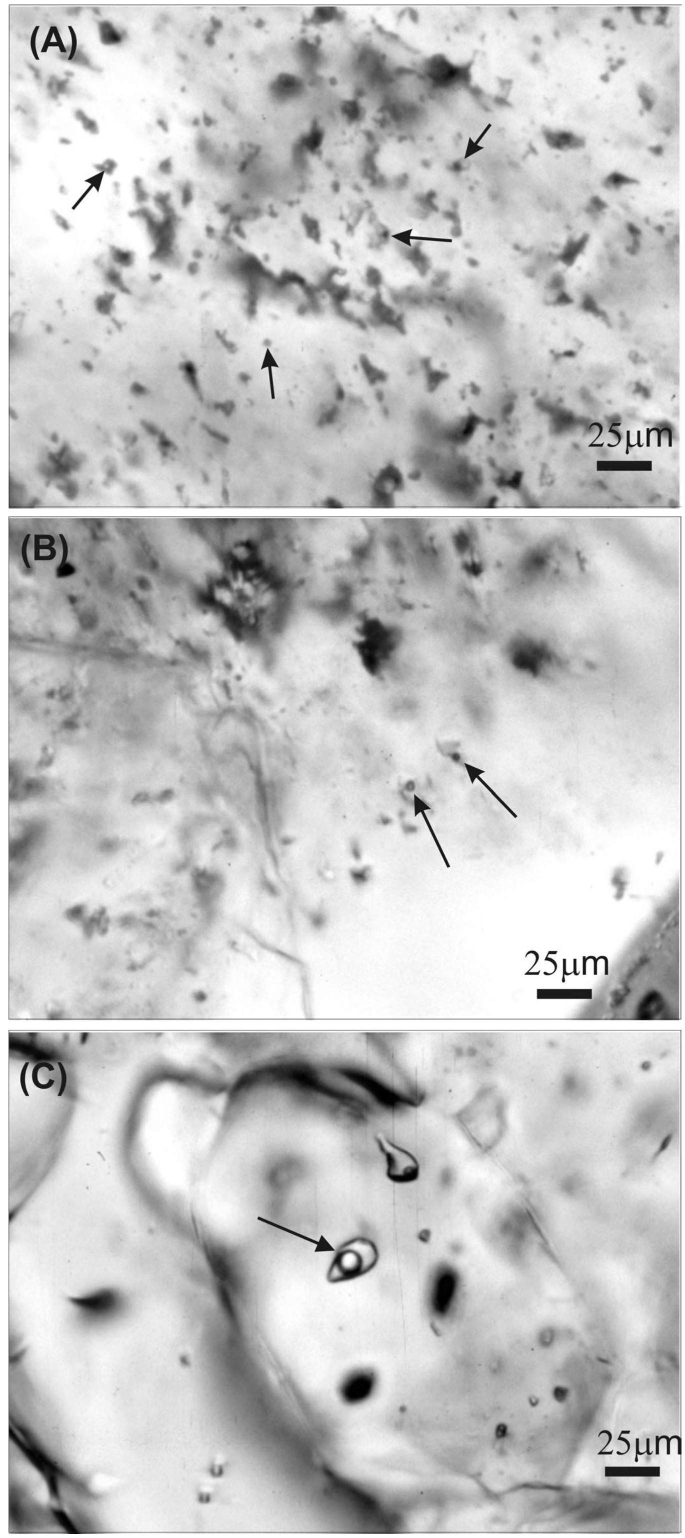

Fig. 5. Photomicrographs showing various occurrences of fluid inclusions, some indicated by arrows on photomicrographs. (**A)** Randomly distributed two-phase aqueous inclusions in RD3. **(B)** Two-phase aqueous fluid inclusions distributed along the edge of a cloudy core of RD3. **(C)** Two-phase gas-oil inclusions in barite.

temperature due to burial ($T_{max\text{-}burial}$) of the Romaine Formation that is based on organic matter reflectance and Lopatin modeling (Bertrand, 1987, 1990). For example, T_h values for the dolomite PD2 are higher (up to 128ºC, Table 1) than $T_{max\text{-}burial}$ in samples from northern Anticosti Island wells such as LGCP (Ro values of 0.85%, $T_{max\text{-}burial}$ of 112ºC; Bertrand, 1990) but similar to $T_{max\text{-}burial}$ of samples from central Anticosti Island wells such as NACP (T_h values for PD2 up to 138ºC) within the gas zone ($T_{max\text{-}burial}$ of 135ºC; Bertrand, 1990). A similar relationship is observed when T_h values of dolomite RD3 (LGCP:T_h = 131ºC, NACP:T_h = 130ºC) is compared with $T_{max\text{-}burial}$ (LGCP = 112ºC, NACP = 135ºC) but the relationship is inverted when T_h values

Table 1. Summary of fluid-inclusion microthermometric data

Sample#	Host Mineral	First-melting Temperature (°C)	Final-melting Temperature	Salinity (wt.%) Range	Salinity Mean	Homogenization Temperature (°C) Range	Homogenization Mean
NACP-40	RD3	-67.2 (1)	-23.8 to -13.6 (3)	17.5 to 23.8 (3)	21.4	71.3 to 116.8 (8)	96.5
	PC2	-68.9 to -66.8 (2)	-36.2 to -26.3(2)	24.7 to 27.4 (2)	25.9	L to 72.2 (3)	
	Barite	-65.0 to -58.5 (2)	-20.4 to -20.1 (3)	21.2 to 22.6 (3)	22.1	L to 110.5 (7)	
NACP-38	PD1		-23.5 to -14.4 (2)	18.1 to 23.7 (2)	20.9	82.9 to 105.1 (5)	96.6
	PC2	-66.9 to -60.0 (3)	-36.4 to -12.0 (9)	16.0 to 27.4 (9)	23.4	60.7 to 120.8 (15)	90.7
						HC: 65.3 to 80.5 (3)	72.8
	Barite	-53.2 to -52.1 (2)	-28.9 to -16.5 (4)	19.8 to 25.2 (4)	22.3	68.1 to 110.6 (5)	91.5
NACP-39	RD3		-20.6 to -8.3 (4)	12.1 to 22.8 (4)	17.8	99.8 to 129.8	109.5
NACP-46	RD3	-56.7 to -56.2 (2)	-20.5 to -10.5 (6)	16.1 to 22.7 (5)	20.2	86.5 to 117.6 (15)	108.5
NACP-44	RD3	-53.1 (1)	-22.4 to -20.4 (2)	22.6 to 23.5 (2)	23.1	83.6 to 113.3 (6)	100.9
	PC2	-62.4 to -58.8 (3)	-29.0 to -20.2 (4)	22.5 to 25.2 (4)	23.8	63.9 to 101.7 (6)	88.2
						HC: 40.0 to 109.5 (10)	86.7
NACP-51	RD3	-68.0 to -53.4 (5)	-29.8 to -17.2 (5)	20.4 to 25.5 (5)	23.2	78.8 to 112.0 (9)	100.2
	PD2	-59.4 to -48.7 (6)	-27.7 to -16.1 (6)	19.5 to 24.8 (6)	22.3	99.2 to 138.4 (13)	120.4
	PC2	-62.4 to -57.0 (2)	-23.6 to -17.2 (3)	20.4 to 23.7 (3)	22.3	60.0 to 100.2 (8)	77.7
	Barite	-71.9 to -68.6 (4)	-32.9 to -20.5 (6)	21.7 to 26.4 (6)	24.9	L to 70.8 (7)	
LGCP-3	PD1		-23.4 to -13.6 (3)	17.5 to 23.7 (3)	20.9	85.1 to 113.3 (8)	97.0
	PC2	-53.9 (1)	-18.0 (1)	20.9 (1)	20.9	78.3 to 93.2 (5)	87.2
LGCP-14	RD2	-58.3 (1)	-25.5 (1)	24.2 (1)	24.2	60.3 to 92.7 (3)	75.9
	RD3	-62.8 to -57.6 (5)	-33.1 to -21.6 (6)	21.9 to 26.5 (6)	24.6	97.8 to 131.3 (9)	110.1
LGCP-18	RD3	-64.2 to -50.7 (4)	-29.8 to -17.1(7)	18.7 to 25.4 (7)	21.8	77.8 to 125.8 (13)	102.7
LGCP-25	PD1	-57.6 to -46.9 (5)	-28.9 to -18.7 (5)	21.4 to 25.2 (5)	23.5	60.3 to 109.3 (11)	89.1
LGCP-26	RD4		-19.7 to -14.7 (4)				
LGCP-24	PD2	-62.6 to -59.2 (3)	-25.6 to -20.9 (5)	22.5 to 24.2 (5)	23.3	106.6 to 127.6 (10)	116.4
LGCP-28	PD2	-64.4 (1)	-32.8 to -30.8 (2)	25.8 to 26.5 (2)	26.2	92.1 to 116.4 (6)	101.5
	PC2	-63.1 to -58.8 (7)	-24.4 to -20.6 (7)	21.3 to 23.4 (7)	22.7	47.2 to 79.3 (14)	62.8
LGCP-31	PC1	-49.8 (1)	-15.6 to -10.8 (3)	14.8 to 19.1 (3)	16.9	34.8 to 77.4 (10)	59.0
	PC2	-60.8 to -59.7 (2)	-23.5 to -23.4 (2)	22.8 to 23.7 (2)	23.4	33.8 to 65.7 (4)	43.4
LGPL-10	RD3	-64.4 (1)	-24.2 (1)	23.9 (1)	23.9	75.6 to 111.3 (3)	89.7
	PD2	-64.5 to -59.6 (4)	-27.3 to -18.9 (5)	21.6 to 24.7 (5)	23.5	96.3 to 137.1 (13)	119.0
QFT-1	RD2	-62.4 to -50.8 (3)	-22.3 to -17.3 (4)	20.4 to 23.4 (4)	22.3	55.6 to 98.2 (12)	74.7
	RD3	-64.2 to -52.5 (8)	-29.2 to -19.3 (10)	21.9 to 25.3 (10)	23.9	59.4 to 114.7 (19)	91.2
CHA-14	RD3	-65.7 to -53.6 (3)	-29.0 to -17.7 (9)	20.9 to 25.2 (9)	21.9	79.1 to 138.5 (11)	101.8
	PD2	-61.3 to -55.8 (3)	-24.5 to -13.1 (10)	17.0 to 23.9 (10)	20.9	113.0 to 150.2 (13)	125.8
CHA-18	RD3		-16.7 (1)	20 (1)	20	70.3 to 118.7 (4)	94.7
	PC2	-57.2 (1)	-23.7 to -20.4 (3)	22.6 to 23.7 (3)	23.2	all-liquid (3)	
CHA-21	RD3	<-44.1	-18.7 to -16.8 (5)	20.1 to 21.4 (5)	20.7	85.9 to 108.9 (5)	93.4
CHA-22	RD3	<-49.1	-20.5 to -17.4 (3)	20.5 to 22.7 (3)	21.6	70.7 to 126.4 (4)	95.6
	PD2	-52.3 (1)	-21.5 to -18.4 (4)	21.2 to 23.3 (4)	22.4	129 to 151 (5)	140.7
	PC2	-65.3 to -53.8 (5)	-33.7 to -29.9 (6)	25.5 to 26.7 (6)	26.1	91.3 to 110.7 (7)	97.1
CHA-32	RD3		-33.4 to -15.7 (3)	19.2 to 26.6 (3)	23.5	93.4 to 123.2 (3)	104.9
	PC1		-17.2 (1)	20.4 (1)	20.4	70.3 (1)	70.3
	PC2		-46.7 to -40.0 (4)	28.2 to 31.3 (4)	29.3	64.7 to 94.2 (4)	80.9
Summary							
	PC1	-49.8 (1)	-17.2 to -10.8 (4)	14.8 to 20.4 (4)	17.8	34.8 to 77.4 (11)	60.0
D1	RD2	-62.4 to -50.8 (4)	-25.5 to -17.3 (5)	20.4 to 24.2 (5)	22.7	55.6 to 98.2 (15)	74.9
	RD3	-68.0 to -44.1 (30)	-33.4 to -8.3 (65)	12.1 to 26.6 (65)	22	59.4 to 138.5 (116)	100.1
D2	RD4	-63.7 to -50.9 (2)	-19.2 to -14.7 (4)	18.4 to 25.5 (4)	22.7	78.3 to 121.5 (9)	92.2
	PD1	-57.6 to -46.9 (5)	-28.9 to -13.6 (10)	17.5 to 25.2 (10)	22.2	60.3 to 113.3 (24)	93.3
D3	PD2	-64.5 to -48.7 (18)	-32.8 to -13.1 (32)	17.0 to 26.5 (32)	22.5	92.1 to 151.0 (61)	120.2
	PC2	-68.9 to -53.8 (27)	-46.7 to -12.0 (41)	16.0 to 31.3 (41)	23.3	33.8 to 120.8 (66)	78.8*
	Barite	-71.9 to -58.5 (6)	-32.9 to -16.5 (13)	19.8 to 26.4 (13)	23.4	51.5 to 110.6 (18)	78.4*

* Liquid inclusions and/or hydrocarbon inclusions are not included.

of dolomite PD1 (LGCP:T_h = 113ºC , NACP:T_h = 105ºC) are compared to $T_{max\text{-}burial}$. It is significant that the diagenetic phases that postdate the D3 event are characterized by lower homogenization temperatures (average of 78.8°C and 78.4°C for late calcite and barite, respectively). However, for the late calcite cement (PC2, Table 1) the T_h values for eastern Anticosti wells, which had shallower paleoburial depths, are significantly lower than those for PC2 cements in the central Anticosti well.

The T_h values clearly support the circulation of a high-temperature fluid responsible for the precipitation of D3 dolomite. The paleoburial depths of the Romaine Formation would have lower $T_{max\text{-}burial}$ and, therefore, did not control the high temperature of the dolomitization fluid. This fluid had temperatures higher than those responsible for the precipitation of the subsequent late calcite and barite cements.

There is no discernible relationship between T_h values and calculated salinities (Fig. 6). Over 90% of salinity values fall within the 17 to 27 wt% $NaCl_{equiv.}$ regardless of their T_h values. Fluids responsible for precipitation of early replacement dolomites to late pore-filling barite cement are all highly saline.

Carbon and Oxygen Stable Isotopes

Because some of the carbonate phases are inseparable by conventional microdrilling, and possibly were formed in similar diagenetic environments, mixtures of known phases of the C1, D1 and D2 events were sampled for stable isotope analyses and interpretation. Analyses of dolomites for the D3 event were done on separated phases (PD1 vs. PD2). The results are listed in Table 2 and illustrated in Figure 8.

Results - Calcite

Eight analyses of the calcite C1 elements (mixtures of SC and RC or PC1) yield $\delta^{18}O$ values from –8.3 to –6.0‰ and $\delta^{13}C$ values from –4.2 to +0.2‰. Seventeen analyses of the C2 phase gave $\delta^{18}O$ values ranging from –14.8 to –5.3‰ and $\delta^{13}C$ from –15.1 to –0.1‰.

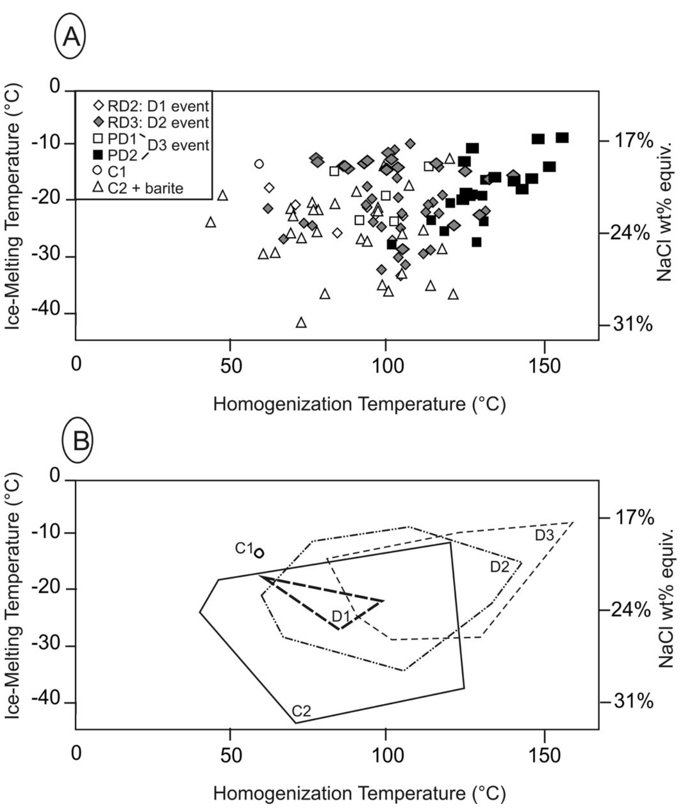

Fig. 6. Homogenization temperature – final ice melting temperature correlation diagram of fluid inclusions in the Romaine Formation. **(A)** The entire dataset for early and late calcites and the dolomite cements. Data are listed in Table 1. **(B)** The fields for the various calcite and dolomite phases in this study.

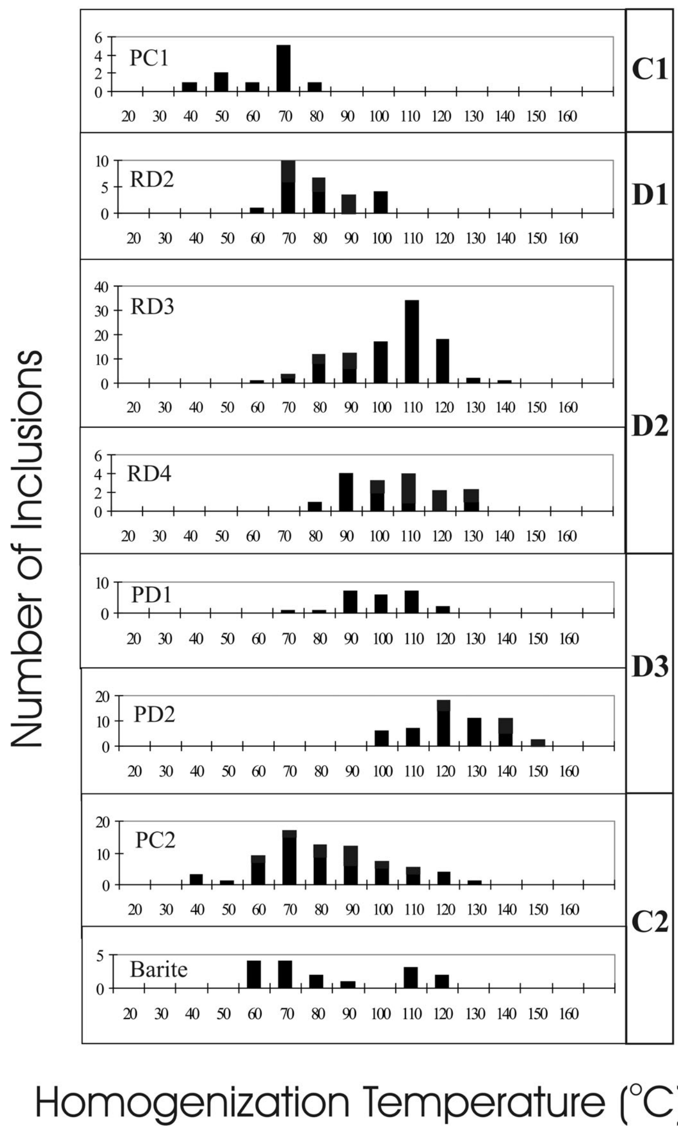

Fig. 7. Histograms of homogenization temperatures of fluid inclusions from various minerals in the Romaine Formation, Anticosti Island and Mingan Islands. Note the progressive increase of average temperature up to a maximum recorded by the second phase of pore-filling dolomite (PD2) followed by a significant decrease in homogenization temperature in the subsequent phases. C1 and C2 - first and second calcitization events, D1, D2 and D3 - first, second and third dolomitization events.

Table 2. Oxygen and Carbon stable isotope ratios for various carbonate phases, and statistical treatment of the data

Sample	Phase	$\delta^{18}O$ (‰) (PDB)	$\delta^{13}C$ (‰) (PDB)
LGCP-33	Calcite 1	-6.8	0.2
LGCP-33	Calcite 1	-6.7	0.2
LGCP-31	Calcite 1	-6.0	-0.3
LGCP-31	Calcite 1	-6.4	-3.0
NACP-25	Calcite 1	-6.2	-1.8
NACP-23	Calcite 1	-6.5	-4.2
LGPL-45a	Calcite 1	-7.0	-2.5
LGPL-12	Calcite 1	-8.3	-2.3
AVERAGE		**-6.7**	**-1.7**
NACP-13	Dolomite 1	-4.0	-3.8
NACP-24	Dolomite 1	-4.7	-2.7
NACP-24	Dolomite 1	-5.3	-3.4
NACP-38	Dolomite 1	-5.3	-0.4
NACP-39	Dolomite 1	-4.4	0.0
NACP-21	Dolomite 1	-5.6	-2.0
NACP-17	Dolomite 1	-4.6	-4.6
NACP-15b	Dolomite 1	-4.4	-3.2
NACP-13a	Dolomite 1	-4.9	-2.6
NACP-13b	Dolomite 1	-5.4	-2.9
NACP-9	Dolomite 1	-4.4	-4.9
NACP-7	Dolomite 1	-5.7	-3.3
NACP-3	Dolomite 1	-5.5	-0.3
NACP-1	Dolomite 1	-5.6	-0.4
LGCP-4	Dolomite 1	-2.0	-0.1
LGCP-3	Dolomite 1	-6.2	-2.8
LGCP-14	Dolomite 1	-8.3	-1.6
LGCP-18	Dolomite 1	-6.0	-0.2
LGCP-25	Dolomite 1	-5.6	-0.5
LGCP-25	Dolomite 1	-5.9	-0.4
LGCP-26	Dolomite 1	-6.1	0.1
LGCP-24	Dolomite 1	-2.9	1.1
LGCP-28	Dolomite 1	-5.5	-0.5
LGCP-27a	Dolomite 1	-5.3	-1.4
LGCP-21-2	Dolomite 1	-6.1	-1.1
LGCP-16a	Dolomite 1	-7.4	-1.4
LGCP-14	Dolomite 1	-6.0	-0.6
LGPL-3	Dolomite 1	-6.3	-3.7
LGPL-10	Dolomite 1	-5.8	-0.1
LGPL-31	Dolomite 1	-5.7	-2.9
LGPL-25	Dolomite 1	-8.5	-2.4
LGPL-18	Dolomite 1	-7.6	-4.0
LGPL-3	Dolomite 1	-7.2	-3.7
LGPL-1	Dolomite 1	-10.8	-3.7
CHA-14-1	Dolomite 1	-5.7	-0.3
CHA-14-2	Dolomite 1	-5.8	0.0
CHA-32	Dolomite 1	-6.3	-2.9
QFT-1	Dolomite 1	-6.1	-1.1
Norsk 86-2	Dolomite 1	-10.9	-1.3
AVERAGE		**-5.9**	**-1.8**

Sample	Phase	$\delta^{18}O$ (‰) (PDB)	$\delta^{13}C$ (‰) (PDB)
NACP-39	Dolomite 2	-5.3	-1.1
NACP-46	Dolomite 2	-5.8	-1.1
NACP-40	Dolomite 2	-5.9	-1.0
NACP-44	Dolomite 2	-5.0	-0.1
NACP-51	Dolomite 2	-5.2	-1.3
NACP-6	Dolomite 2	-5.6	-0.6
NACP-4	Dolomite 2	-7.5	-2.1
LGCP-14	Dolomite 2	-7.6	-1.5
LGCP-18	Dolomite 2	-5.8	-0.2
LGCP-26	Dolomite 2	-5.8	-0.2
LGCP 27b	Dolomite 2	-4.5	-1.1
LGCP-26	Dolomite 2	-5.9	-0.3
LGCP-24	Dolomite 2	-5.9	-0.4
LGCP-16b	Dolomite 2	-6.2	-1.0
LGCP-8	Dolomite 2	-8.1	-3.2
LGCP-1	Dolomite 2	-7.0	-2.8
LGPL-10	Dolomite 2	-6.4	-0.3
LGPL-45b	Dolomite 2	-7.9	-2.4
LGPL-6a	Dolomite 2	-8.5	-4.1
QFT-1	Dolomite 2	-7.4	-1.2
Norsk 86-2	Dolomite 2	-6.3	-0.9
Norsk 86-3	Dolomite 2	-6.2	-0.8
Norsk 86-3	Dolomite 2	-6.8	-1.0
Norsk 86-4	Dolomite 2	-7.0	-1.2
AVERAGE		**-6.4**	**-1.2**
NACP-19	Dolomite 3	-4.4	-3.9
NACP-15a	Dolomite 3	-8.4	-5.0
LGCP-3	Dolomite 3	-6.4	-2.7
LGCP-25	Dolomite 3	-8.9	-0.6
LGCP-24	Dolomite 3	-8.5	-0.5
LGCP-25	Dolomite 3	-5.8	-0.2
LGPL-10	Dolomite 3	-8.7	-0.8
LGPL-37	Dolomite 3	-10.2	-3.5
LGPL-6	Dolomite 3	-13.8	-4.8
Norsk 86-2	Dolomite 3	-6.6	-0.9
Norsk 86-3	Dolomite 3	-7.2	-0.9
AVERAGE		**-8.1**	**-2.2**

Sample	Phase	$\delta^{18}O$ (‰) (PDB)	$\delta^{13}C$ (‰) (PDB)
NACP-44	Calcite 2	-10.1	-2.7
NACP-51	Calcite 2	-10.2	-2.9
NACP-14	Calcite 2	-9.3	-4.0
NACP-10	Calcite 2	-7.4	-11.6
NACP-5	Calcite 2	-10.5	-2.9
NACP-2	Calcite 2	-6.8	-2.4
LGCP-28	Calcite 2	-9.8	-2.2
LGCP-31	Calcite 2	-7.9	-15.1
LGCP-18	Calcite 2	-8.0	-3.7
LGCP-9-4	Calcite 2	-5.3	-1.9
LGPL-45	Calcite 2	-6.4	-3.1
LGPL-42	Calcite 2	-6.2	-2.7
LGPL-40	Calcite 2	-5.9	-1.7
LGPL-22	Calcite 2	-8.7	-3.6
LGPL-17	Calcite 2	-14.8	-2.8
LGPL-16	Calcite 2	-7.6	-3.3
Norsk 86-3	Calcite 2	-9.0	-0.1
Norsk 86-4	Calcite 2	-10.2	-2.6
Norsk 86-5	Calcite 2	-12.2	-2.1
AVERAGE		**-8.8**	**-3.8**

LEGEND for statistical tables
Std. Dev: Standard deviation
#: Number of samples
ORD. Mar. Dol.: Ordovician marine dolomite
t Student: value of the Student's statistic test
t table 95%: 95% confidence value
df1 and df2: degree of freedom for the parameter

$\delta^{13}C$ (‰) (PDB)		**D1/Marine dolomite**		
Average	-1.8	Ord. Mar. Dol.		-2
Maximum	1.1	t Student=		**0.80**
Minimum	-4.9	t table 95%		2.021
Std. Dev.	1.6	**Not significant**		
#	39			

$\delta^{18}O$ (‰) (PDB)		**D1/Marine dolomite**		
Average	-5.9	Ord. Mar. Dol.		-4.5
Maximum	-2.0	t Student=		**-5.12**
Minimum	-10.8	t table 95%		-2.021
Std. Dev.	1.7	**Very**	>>1:1000	
#	39	**Significant**		

$\delta^{18}O$ (‰) (PDB)					**D2/D1**		
Average	-6.4	Ord. Mar. Dol.		-4.5	t'=	**1.4**	**Not significant**
Maximum	-4.5	t Student=		**-8.21**	t' table 95%	2.04	
Minimum	-8.5	t table 95%		-2.06	df1	38	
Std. Dev.	1.1	**Very**	>>1:1000		df2	23	
#	24	**Significant**			t1 table	2.021	
					t2 table	2.069	

$\delta^{18}O$ (‰) (PDB)					**D3/D1**			**D3/D2**		
Average	-8.1	Ord. Mar. Dol.		-4.5	t'=	**2.72**	**Significant >1:20**	t'=	**2.12**	**Not significant**
Maximum	-4.4	t Student=		**-4.73**	t' table 95%	2.20		t' table 95%	2.21	
Minimum	-13.8	t table 95%		-2.228	df1	38		df1	23	
Std. Dev.	2.5	**Very**	>>1:1000		df2	10		df2	10	
#	11	**Significant**			t1 table	2.021		t1 table	2.069	
					t2 table	2.228		t2 table	2.228	

Results - Dolomite

Thirty-six analyses of the D1 elements (mixtures of RD1 and RD2 or pure RD2) show similar $\delta^{18}O$ and $\delta^{13}C$ values. Except for two divergent values ($\delta\,^{18}O$ and $\delta\,^{13}C$ of –10.8‰ and –4.9‰, and –10.9‰ and –1.3‰, respectively), $\delta^{18}O$ and $\delta^{13}C$ values of D1 are in the range from –8.5 to –2.0‰, and from –4.0 to +1.1‰, respectively. Twenty-two analyses of the D2 elements (RD3 and RD4) gave $\delta^{18}O$ and $\delta^{13}C$ values ranging from –8.5 to –4.5‰, and –4.1 to –0.1‰, respectively. Eleven analyses of the D3 elements (PD1 and PD2) gave $\delta^{18}O$ values ranging from –13.8 to –4.4‰ and $\delta^{13}C$ from –5.0 to –0.2‰.

Interpretation of Diagenetic Fluids Recorded in Romaine Formation

The first calcite (C1)

The $\delta^{18}O$ and $\delta^{13}C$ values for C1 elements are consistent with the ranges of Early Ordovician marine calcite ($\delta^{18}O$ ranging from –8.4 to –8.9‰ and $\delta^{13}C$ ranging from –2.5 to –0.7‰; Qing and Veizer, 1994; Fig. 8). The fluid inclusion T_h values for the early pore-filling calcite (PC1) are the lowest of our data set (35 ºC to 77 ºC). Petrographic and geochemical data suggest that the C1 phases were either deposited in the sedimentary environment (SC) or formed in near surface diagenetic environments (RC and PC1).

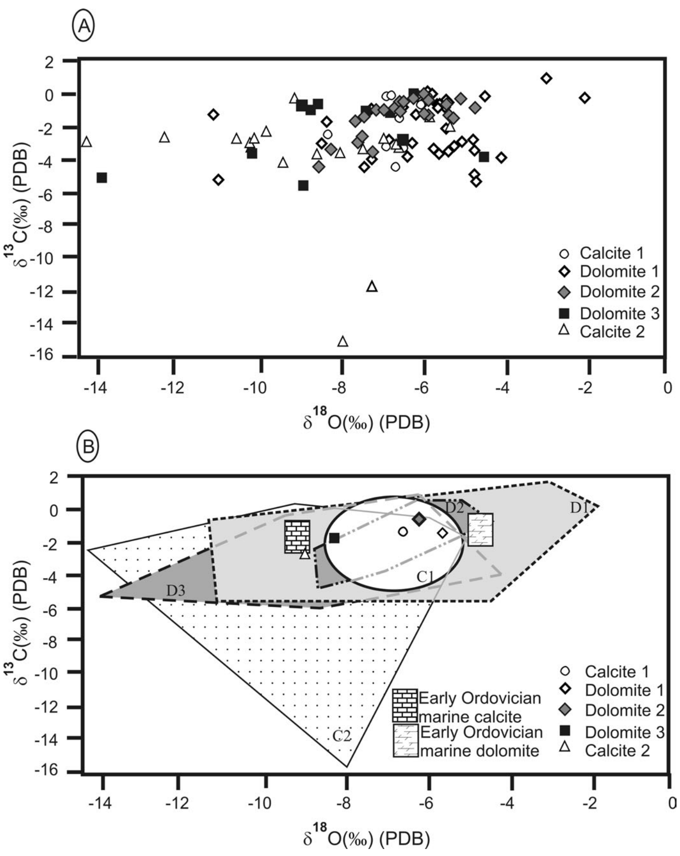

Fig. 8. (A) Cross-plot of individual oxygen and carbon stable isotope ratios of various calcite and dolomite phases in the Romaine Formation. Data are listed in Table 2. **(B)** Fields for the various calcite and dolomite phases in this study with an average for each type of carbonates. The Lower Ordovician marine calcite and marine dolomite fields are from Qing and Veizer (1994).

The first dolomite (D1)

From the published $\delta^{18}O$ values of marine calcites (average of –8.5‰) and the +4‰ assumed difference between calcite and dolomite (Veizer, 1983), the average $\delta^{18}O$ value of Early Ordovician marine dolomite is expected to be around –4.5‰. Therefore, the D1 event (RD1 and RD2) is slightly to moderately depleted in ^{18}O ($\delta^{18}O$ average of –5.8‰) with respect to marine dolomite (probability for similarity less than 1:10000 according to Student’s t test, Table 2, Snedecor and Cochran, 1978). This indicates either (1) precipitation from a marine-derived fluid at slightly higher temperature in shallow burial condition, or (2) some recrystallization of a marine or very shallow burial dolomite precursor in the presence of a relatively higher temperature fluid. The moderately high T_h (55–98°C) and high salinity (20.4 to 24.2 wt% $NaCl_{equiv.}$) values of fluid inclusions are more consistent with recrystallization of a dolomite precursor in the presence of a high temperature and saline fluid that was incorporated later in the diagenetic system.

A few RD1 and RD2 samples are clearly depleted in ^{13}C ($\delta^{13}C$ from –4.9 to –3.8‰) with respect to marine carbonates (Fig. 8). This suggests that some of the recrystallization occurred in the presence of significantly ^{13}C-depleted diagenetic fluid and could indicate the presence of a large volume of biogenic HCO_3^- that could be derived from thermochemical sulphate reduction of organic matter (Machel, 1987).

The second dolomite (D2)

The $\delta^{18}O$ values of D2 elements (RD3 and RD4) largely overlap with those of the D1 event. The average $\delta^{18}O$ value of D2 dolomites (–6.3‰) is slightly more depleted in ^{18}O than D1 (–5.8‰), however, the statistical Student’s test indicates that this difference is not significant (Table 2). This could suggest that D2 dolomites were formed at slightly higher temperatures than the D1 phase. However, this would translate into a slight increase of roughly 3ºC and since the T_h values of D2 (59–139°C, average of 99ºC) are significantly higher than that of D1 (55–98ºC, average of 75ºC), an influx of slightly ^{18}O-depleted but still highly saline fluid (12–26.6 wt% $NaCl_{\ equiv.}$) might be recorded in the D2 phase.

The third dolomite (D3)

The range of $\delta^{18}O$ values of D3 dolomites shows significant overlap with the D1 and D2 fields. However, there is a large number of $\delta^{18}O$ values for D3 that are significantly more depleted (less than –8.3‰) compared to the earlier D1 and D2 events, with an average 2.0‰ difference between D2 and D3 dolomite ratios (Fig. 8). This likely indicates that locally D3 pore- and fracture-filling dolomite precipitated out of a high temperature and highly saline (17.0–26.5 wt% $NaCl_{\ equiv.}$) fluid. The scattered $\delta^{18}O$ values indicate precipitation over a wide range of temperatures. This wide temperature range is well supported by the variability of T_h values for the dolomite phase

(60–151°C, average of 111ºC). The 2.0‰ average difference in $\delta^{18}O$ values between D2 and D3 would translate into an average increase of roughly 12ºC in precipitation temperature, assuming an isotopically similar diagenetic fluid for D2 and D3. This agrees well with the difference in average T_h values between D2 (99ºC) and D3 (111ºC) dolomites.

The late calcite (C2)

The $\delta^{18}O$ values of calcite C2 are as variable as, and commonly overlap with, values for the D3 dolomites, again suggestive of a wide range of temperature of precipitation. Given the +4‰ difference between calcite and dolomite, the significant overlap between calcite and dolomite $\delta^{18}O$ values indicates that the conditions were cooler during precipitation of the late calcite, assuming a common fluid for precipitation. This conclusion is supported by the lower T_h values recorded by fluid inclusions in the C2 calcites (34–121°C, average of 79ºC). The overall decrease in precipitation temperatures is also supported by the T_h values of the post-C2 barite cement (51.5–110.6ºC, average of 78ºC). The C2 and barite fluid inclusions are also characterized by high salinity values (average of 23.3 and 23.4 wt% NaCl $_{equiv.}$, respectively), which supports the interpretation of a common fluid for precipitation of D3 dolomite and C2 calcite and barite cements. Two C2 samples are very depleted in ^{13}C ($\delta^{13}C$ of –11.6 and –15.1‰) with respect to marine carbonates (Fig. 8). This suggests that precipitation of some late calcite cements occurred in the presence of $\delta^{13}C$-depleted diagenetic fluid, and indicates the presence of a significant volume of hydrocarbon-derived HCO_3^- in the fluid. These late calcites commonly host hydrocarbon fluid inclusions, further supporting the interpretation of the presence of hydrocarbons in the late diagenetic fluid system.

The important decrease in T_h values from the D3 event to the late PC2 and barite phases indicates a significant change in the thermal regime recorded by the Romaine Formation after the regional high temperature fluid event that resulted in the brecciation, leaching, alteration and dolomitization (D2 to D3 events) of the Lower Ordovician carbonates (Figs. 4, 7). According to Bertrand's (1987, 1990, 1991) organic matter maturation values ($R_{o\ (vi\text{-}eq)}$ values range from 0.85% to 2.4% from northeast to southwest Anticosti wells) and suggested burial temperatures (112ºC to 168ºC from northeast to southwest wells), the precipitation of the PC2 and barite cements occurred at temperatures lower than those of maximum burial. The precipitation of the late phases occurred after some significant time break to allow for either a regional decrease in geothermal gradient or perhaps tectonically-controlled uplift of the Anticosti Basin. Modelling by Bertrand (1990) suggested that hydrocarbon generation peaked at the end of the Early Devonian. Uplift that could be related to the Middle Devonian Acadian Orogeny (Bertrand and Malo, 2001) might explain the lower T_h values in the latest diagenetic phases.

The high temperature fluids recorded by the D2 and D3 dolomites may have been derived from pulses of overpressured fluids from the central part of the Anticosti Basin (Chi et al., work in progress), where the temperature of the fluids may have been equal to the maximum burial temperature. Therefore, the D2–D3 event dolomites would be burial-related rather than hydrothermal (*sensu stricto*) there. In the marginal part of the basin, however, where the fluid temperature is higher than maximum burial temperature (e.g., LGCP / Chaloupe wells, D3 dolomite T_h up to 151ºC versus $T_{max\text{-}burial}$ of 112ºC), due to rapid fluid advection, the dolomite would be hydrothermal. The differential temperature between hydrothermal dolomite and background in the Romaine Formation shows more subtle variations when compared to literature examples where the fluid temperature is significantly higher than the background maximum (e.g., Lavoie and Morin, 2004).

Hydrothermal Alteration of the Romaine Formation

The recognition of hydrothermal alteration of carbonates is commonly based on combined macroscopic, microscopic and geochemical evidence (Al-Aasm, 2003; Lavoie and Morin, 2004; Davies, 2004).

Macroscopic evidence

Studies of Paleozoic hydrothermal dolomite reservoirs have documented a number of large scale features commonly associated with hydrothermal alteration of a carbonate host (Hurley and Budros, 1990; Boreen and Davies, 2004). A critical element is the presence of active extensional and/or transtensional faults that act as potential conduits for the advective circulation of high temperature fluids.

Fault control on sedimentary thickness

Thicker sedimentary successions occur on the downthrown blocks of extensional faults in other regional hydrothermal dolomite systems (e.g., Lavoie and Morin, 2004). From core study, the Romaine Formation is characterized by anomalously thicker sedimentary successions southwest (downthrown block) of the major Jupiter fault (Fig. 1; Lavoie, 1997a; Chi and Lavoie, 2001).

Other smaller-scale extensional faults in the study area are seen on the seismic profiles (Roksandic and Granger, 1981; Lynch and Trollope, 2001; Castonguay et al., 2005). These faults were episodically active from the Arenigian (Romaine) until the end-Caradocian (lower part of Vauréal), a time interval roughly coincident with the main phase of Taconian accretion at the outboard margin of Laurentia (van Staal et al., 1998). These extensional faults are the likely distal foreland expression of the building orogenic wedge (Bradley and Kidd, 1991). A similar relationship was described from coeval strata in nearby western Newfoundland (Stenzel et al., 1990) and southern Quebec (Lavoie, 1994). These seismic profiles also locate other areas where thickness increases in the Romaine Formation are associated with faults.

Collapse of brecciated segments of carbonate platform

The association of collapsed fault-bounded segments of a carbonate platform and potential hydrothermal dolomite hydrocarbon reservoirs has long been considered to be an exploration guide. Extensional faulting will lead to brecciation and collapse of segments of the carbonate platform, hydrothermal fluids will use this new permeability framework to circulate in the platform units resulting in carbonate dissolution and associated partial dolomite cementation of vug space and replacement of precursor carbonates. The collapse is rarely visible in field outcrops (Lavoie, 2005a) and its seismic expression is subtle and commonly seen as disruption in the continuity of seismic markers (Hurley and Budros, 1990). Recent seismic data across Anticosti Island show clearly fault-bounded collapsed segments from the Romaine Formation to the top of the Mingan Formation as well as significant loss of seismic marker continuity (Lynch and Trollope, 2001).

Microscopic evidence

Migration of high-temperature diagenetic fluids commonly leads to dissolution and corrosion of the precursor host, localized to pervasive dolomitization and an almost universal paragenetic suite of base metal sulphides, saddle dolomite, ± bitumen, calcite and calcium sulphate (Smith, 2004).

Dolomite is common in the intertidal and subtidal facies of the Romaine Formation. In fifth-order, metre-thick shallowing-upward cycles (Lavoie, 1997a, b), the subtidal facies are pervasively dolomitized (RD2 and RD3) when these fifth-order cycles are part of the intertidal-dominated (regressive phase) segments of larger-scale third-order cycles (Lavoie, 1997a). For intervals dominated by subtidal facies (base of third-order cycles) dolomite is minor on Anticosti Island, although similar but commonly thinner subtidal-dominated cycles on the Mingan Islands and adjacent mainland are pervasively dolomitized.

An empirical relationship exists between pervasive early (shallow burial) dolomitization and abundant intertidal facies; for example, in the (1) Upper Knox Group of southern U.S. Appalachians (Read, 1989; Montañez and Read, 1992; Montañez, 1994); (2) St. George Group of western Newfoundland (James et al., 1989); and (3) Beekmantown Group of the southern Quebec Appalachians (Bertrand et al., 2003; Salad Hersi et al., 2003). The subtidal-dominated segments of third-order cycles are dolomitized to a minor extent, if at all, compared to the intertidal-dominated segments developed during the regressive phase of the third-order cycles. However, pervasive dolomitization of all intertidal and subtidal facies is observed for some stratigraphically thinner successions on the basin margins (Desrochers, 1985; Salad Hersi et al., 2003). Brecciation and early pervasive dolomitization appear to have been critical elements in focusing some high temperature fluid flow into the carbonate host to develop major secondary porosity (e.g., Bertrand et al., 2003).

Lower Ordovician carbonates in eastern North America (e.g., Ellenburger - Loucks and Anderson, 1985; Arbuckle - Raymond and Osborne, 1991; St. George - Cooper et al., 2001; Beekmantown - Bertrand et al., 2003) are typically hydrothermal dolomite plays with saddle dolomite precipitated from high-temperature, saline fluids (Radke and Mathis, 1980; Al-Aasm, 2003). Saddle dolomite is ubiquitous in the Lower Ordovician Romaine Formation, either as a vug- and fracture-filling cement or as a replacement of previous carbonate. Saddle dolomite in the Romaine Formation is intimately associated with minor sphalerite (MVT-type) mineralization, and is commonly succeeded by an almost invariable succession of calcite followed by sulphate. Bitumen sometimes immediately postdates the saddle dolomite.

Geochemical evidence

Hydrothermal alteration of a carbonate unit leaves a geochemical imprint, which helps to recognize the process. Saddle dolomite is commonly characterized by (1) significantly- to slightly-depleted $\delta^{18}O$ and $\delta^{13}C$ values compared to coeval seawater-derived carbonates and earlier diagenetic products; (2) a wide range of intermediate to very high T_h values (100–200ºC) for fluid inclusions that are commonly higher than the estimates of coeval and even maximum burial temperatures; (3) commonly highly saline (>20 wt% $NaCl_{equiv.}$) fluid inclusions (with some exceptions); and (4) radiogenic $^{87}Sr/^{86}Sr$ values compared to coeval marine values (Al-Aasm, 2003; Smith, 2004). The wide range of fluid inclusion homogenization temperatures and $\delta^{18}O$ values in saddle dolomite results from the highly fluctuating physical and chemical properties of the hydrothermal fluids which travel vertically and laterally through the host rock, and precipitate dolomites over a wide range of temperatures as the fluid cools and rock/water ratios evolve (Smith, 2004).

The saddle dolomites of the Romaine Formation (PD1 and PD2) are characterized by a wide range of both T_h and $\delta^{18}O$ values. However, PD1 and PD2 dolomites also have the highest T_h values and most depleted $\delta^{18}O$ values of the entire dataset. High T_h and depleted $\delta^{18}O$ values are particularly significant for wells and outcrops near the northern erosional edge of the basin where paleoburial depth and temperatures were independently shown (Bertrand, 1987, 1990) to be lower than that of fluid inclusions in the D3 saddle dolomite (see fluid inclusion section earlier in text). It is also noteworthy that earlier replacement dolomites (D2 event) are also characterized by some high T_h values, that suggest that some alteration and recrystallization of these earlier dolomites occurred in the presence of high temperature fluids. As with the observation for the D3 dolomites, this fact is significant for the circulation of hydrothermal fluids in the northern part of the Anticosti basin (see RD3 dolomite in LGCP and Chaloupe wells, Table 1).

Hydrocarbon Migration in the Romaine Formation: Reservoir Potential

The above discussion indicates that subtidal and intertidal facies in the Romaine Formation in the northern part of the Anticosti Island basin were strongly altered by diagenetic fluids that were likely hydrothermal in origin. Hydrothermal fluids migrated in the carbonates and the migration was enhanced through fault-related fracturing / brecciation of the Romaine Formation. Leaching of the carbonate host was significant as secondary porosity is visible in all studied cores, locally reaching up to 30% over metre-scale intervals, based on visual estimates (Lavoie, 1997a, b, 1998). The carbonate succession experienced multiple events of partial cementation (saddle dolomite, calcite, sulphate) interrupted by repetitive dissolution seen in D2 and D3 dolomites.

In the secondary permeability framework, migration of hydrocarbons is recorded by (1) the presence of bitumen coating some pore spaces or saddle dolomite crystals; (2) hydrocarbon fluid inclusions in the late pore-filling calcite and barite cements; and (3) reports of bleeding oil and gas shows from the Romaine intervals in most old as well as recent drill holes (MRN, 1974; Lavoie, 1997a, b; Lynch and Trollope, 2001; Lynch and Grist, 2002). The hydrocarbons were derived from the Macasty Formation, which lies above the Mingan Formation. Downward migration was driven by significant fluid overpressure developed within the source rocks in the structurally lower southern central part of the basin (Chi et al., work in progress). The timing of primary hydrocarbon migration is unknown, but likely occurred during or after the Early Devonian during the period of oil generation (Bertrand, 1990) and when overpressures reached their maximum.

The Ordovician–Silurian strata on Anticosti Island forms a southwesterly-dipping homoclinal succession without significant folds. Lateral and vertical diagenetic closures formed by the transition from porous dolostone reservoir to a tight non-porous dolostone / limestone encasing succession could provide a trapping mechanism for migrating hydrocarbons. Moreover, the major Sauk–Tippecanoe sequence-bounding unconformity at the top of the Romaine Formation could also have provided an upper migration barrier if not breached by extensional faults.

Conclusions

Petrographic, fluid-inclusion and stable isotope data indicate that there are several types of dolomites in the Romaine Formation, ranging from early diagenetic to late-stage hydrothermal. Early diagenetic dolomitization (D1 event) did not create porosity, whereas significant porosity was produced during the D2 and D3 dolomitization events associated with high temperature, highly saline fluids that can be qualified as hydrothermal in the northern erosional edge of the Anticosti Basin. The occurrence of oil inclusions in late calcite cement and barite indicates petroleum migration after the formation of dolomitization-related porosity.

The high temperature, hydrothermal alteration event was of regional scale, as its physical characteristics (secondary porosity, saddle dolomite–late calcite–sulphate cements) and geochemical expressions (high homogenization temperatures and high salinities of fluid inclusions) are noted in all cored intervals of the Romaine Formation. These petrographic and geochemical attributes combine with the other geological (fault-controlled thickness increase) and geophysical (seismic sag and loss of reflectors) evidence to support the interpretation that the Lower Ordovician carbonates of Anticosti Island were hydrothermally altered. The secondary porosity framework generated during dolomitization subsequently allowed hydrocarbon migration.

Acknowledgments

We thank Shell Canada, Encal Energy and Corridor Resources for significant support at various stages of this research. We are grateful to Hairuo Qing for his initial review of the manuscript which also benefited from in depth reviews, and we appreciated comments from Bulletin reviewers Graham Davies and Mario Coniglio as well as from Bulletin editor Glen Stockmal. The Natural Sciences and Engineering Research Council of Canada, the Natural Resources of Canada National Geoscience Mapping (NATMAP) Program and the Targeted Geoscience Initiative program all provided past and on-going research support. The Ministère des Ressources Naturelles et de la Faune du Québec allowed for access to cores from Anticosti Island. Geological Survey of Canada contribution number 2004471.

References

Achab, A. 1977. Les chitinozoaires de la Zone à *Dicellograptus complanatus* Formation de Vauréal, Ordovicien supérieur, Ile d'Anticosti, Québec. Canadian Journal of Earth Sciences, v. 14, p. 413-425.

_____ 1978. Sur quelques chitinozoaires de la Formation Vauréal et de la Formation Macasty (Ordovicien supérieur), Ile d'Anticosti, Québec, Canada. Review of Paleobotany and Palynology, v. 25, p. 295-314.

_____ 1989. Ordovician chitinozoan zonation of Quebec and Western Newfoundland. Journal of Paleontology, v. 63, 14-24.

Al-Aasm, I. 2003. Origin and characterization of hydrothermal dolomite in the Western Canada Sedimentary Basin. Journal of Geochemical Exploration, v. 78-79, p. 9-15.

Barnes, C.R. 1984. Early Ordovician eustatic events in Canada. In: Bruton, D.L. (ed.). Aspects of the Ordovician System: Paleontological Contributions from the University of Oslo #295, Universitetsforlaget, p. 51-63.

Bertrand, R. 1987. Maturation thermique et potentiel pétroligène des séries post-taconiennes du nord-est de la Gaspésie et de l'île d'Anticosti. Doctorate thesis, Université de Neufchâtel, Suisse, 647p., http://www.unine.ch/biblio.

_____ 1990. Maturation thermique et histoire de l'enfouissement et de la génération des hydrocarbures du bassin de l'archipel de Mingan et de l'Île d'Anticosti. Canadian Journal of Earth Sciences, v. 27, p. 731-741.

_____ 1991. Maturation thermique des roches-mères dans les bassins des basses-terres du Saint-Laurent et dans quelques buttes témoins au sud-est du Bouclier canadien. International Journal of Coal Geology, v. 19, p. 359-383.

_____ and Héroux, Y. 1987. Chitinozoan, graptolite, and scolecodont reflectance as an alternative to vitrinite and pyrobitumen reflectance in Ordovician and Silurian strata, Anticosti Island, Quebec, Canada. American Association of Petroleum Geologists Bulletin, v. 71, p. 951-957.

_____ and Malo, M. 2001, Source rock analysis, thermal maturation, and hydrocarbon generation in the Siluro-Devonian rocks of the Gaspé Belt basin. Canada. Bulletin of Canadian Petroleum Geology, v. 49, p. 238-261.

_____, Chagnon, A., Duchaine, Y., Lavoie, D., Malo, M. and Savard, M.M. 2003. Sedimentologic, diagenetic and tectonic evolution of the Saint-Flavien gas reservoir at the structural front of the Quebec Appalachians. Bulletin of Canadian Petroleum Geology, v. 51, p. 126-154.

Boreen, T. and Davies G.R. 2004. Hydrothermal dolomite and leached limestones in a TCF gas play: the Ladyfern Slave Point reservoir NEBC. Dolomites: The spectrum – Mechanisms, Models, Reservoir Development. January 13–15, 2004 Meeting in Calgary, extended abstracts on CD-Rom.

Bradley, D.C. and Kidd, W.S.F., 1991. Flexural extension of the upper continental crust in collisional foredeeps. Geological Society of America Bulletin, v. 103, p. 1416-1438.

Brennan-Alpert, P. 2001. Regional deposition and diagenesis of Lower Ordovician epeiric, platform carbonates : the Romaine Formation, Mingan Archipelago and Subsurface Anticosti Island, Eastern Quebec. M.Sc. thesis, University of Ottawa, Ottawa, Ontario.

Castonguay, S., Wilson, R.A, Brisebois, D., Desrochers and A., Malo, M. 2005, Compilation géologique, Anticosti-Gaspé-Campbellton, Les ponts géologiques de l'est du Canada, Transect 4, Québec – Nouveau-Brunswick. Geological Survey of Canada, Open File 4883, 1/125 000 , 4 sheets.

Chi, G., Bertrand, R. and Lavoie, D. 2000. Regional-scale variation of characteristics of hydrocarbon fluid inclusions and thermal conditions along the Paleozoic Laurentian continental margin in eastern Quebec, Canada. Bulletin of Canadian Petroleum Geology, v. 48, p. 193-211.

_____ and Lavoie, D. 2001. A diagenetic study of dolostones of the Lower Ordovician Romaine Formation, Anticosti Island. Geological Survey of Canada, Current Research 2001-D17, 13p.

_____, _____ and Lynch, G. 2001. Petrographic and geochemical study of dolostones in the Trenton Formation from the Chaloupe Well, Anticosti Island, with comparison to dolostones of the Romaine Formation. Internal report to Shell Canada, 30p.

Copper, P. 1981. Atrypoid brachiopods and their distribution in the Ordovician-Silurian sequence of Anticosti Island. In: Subcommission on Silurian Stratigraphy, Ordovician-Silurian Boundary Working Group. Field Meeting, Anticosti-Gaspé, 1981. Volume II, Stratigraphy and Paleontology. P. J. Lespérance (ed.). Université de Montréal, Montréal, Québec, p.137-141.

Cooper, M., Weissenberger, J., Knight, I., Hostad, D., Gillespie, D., Williams, H., Burden, E., Porter-Chaudhry, J., Ray, D. and Clark, E. 2001. Basin evolution in western Newfoundland: New insights from hydrocarbon exploration. American Association of Petroleum Geologists Bulletin, v. 85, p. 393-418.

Davies, G.R. 2004. Hydrothermal (thermobaric) dolomitization: rock fabric and organic petrology support for emplacement under conditions of thermal transients, shear stress, high pore fluid pressure with abrupt pressure transients, hydro fracturing, episodic rapid fluid flow, and instantaneous cementation by saddle dolomite. In: Dolomites: the spectrum, mechanisms, models, reservoir development. G.R. Davies, J. Packard and R.McAuley (eds.). Canadian Society of Petroleum Geologists, Special Publication 63, abstracts on CD-Rom.

_____ 2005. Hydrothermal dolomite and leached limestone reservoirs: tectonic, structural, mining and petroleum geology linkage. American Association of Petroleum Geologists / Canadian Society of Petroleum Geologists, Joint Annual Meeting, Calgary 2005. Program with abstracts.

Desrochers, A. 1985. The Lower and Middle Ordovician platform carbonates of the Mingan Islands, Quebec : Stratigraphy, sedimentology, paleokarst, and limestone diagenesis. Ph.D. thesis, Memorial University of Newfoundland, Newfoundland, 454p.

_____ and James, N.P. 1988. Early Paleozoic surface and subsurface paleokarst: Middle Ordovician Carbonates, Mingan Islands, Quebec. In: Paleokarst. N.P. James and P.W. Choquette (eds.). Springer-Verlag, p. 183-210.

Dickson, J.A. 1966. Carbonate identification and genesis as revealed by staining. Journal of Sedimentary Petrology, v. 36, p. 491-505.

Eaton, S. 2004a. Tracking a play without border: Canadians eye the prolific Trenton. American Association of Petroleum Geologists, Explorer, February 2004.

_____ 2004b. Looking for new found oil in Newfoundland: Structure, dolomites look good. American Association of Petroleum Geologists, Explorer, March 2004.

_____ 2004c. Hydrothermal dolomite ideas sparks play: Zebra hunt may lead to elephants. American Association of Petroleum Geologists, Explorer, April 2004.

Goldstein, R.H. and Reynolds, T.J. 1994. Systematics of fluid inclusions in diagenetic minerals. Society of Economic Paleontologists and Mineralogists Short Course 31, 199p.

Hurley, N.F. and Budros, R. 1990. Albion-Scipio and Stoney Point fields – USA Michigan Basin. In: Stratigraphic traps 1. E.A. Beaumont and N.H. Foster (eds.). American Association of Petroleum Geologists, Treatise of Petroleum Geology, Atlas of Oil and Gas fields, p. 1-38.

Jacobi, R.D. 1981. Peripheral bulge – A causal mechanism of the Lower/Middle Ordovician unconformity along the western margin of the northern Appalachians. Earth and Planetary Science Letters, v. 56, p. 245-251.

James, N.P., Stevens, R.K., Barnes, C.R. and Knight, I. 1989. Evolution of a Lower Paleozoic continental-margin carbonate platform, northern Canadian Appalachians. In: Controls on Carbonate Platform and Basin Development. P.D. Crevello, J.L. Wilson, J.F. Sarg and J.F. Read (eds.). Society of Economic Paleontologists and Mineralogists Special Publication 44, p. 123-146.

Kesler, S.E. 1994. Mississippi Valley-type deposits in continental margin basins: lessons from the Appalachian-Caledonian orogen. In: Sediment-hosted Zn-Pb ores. L. Fotebote and M. Boni (eds.). Springer-Verlag p. 89-103.

Knight, I., James, N.P. and Lane, T.E. 1991. The Ordovician St. George Unconformity, northern

Appalachians: The relationship of plate convergence at the St. Lawrence Promontory to the Sauk-Tippecanoe sequence boundary. Geological Society of America Bulletin, v. 103, p. 1200-1225.

Lavoie, D. 1994. Diachronous tectonic collapse of the Ordovician continental margin, eastern Canada: comparison between the Quebec Reentrant and the St. Lawrence Promontory. Canadian Journal of Earth Sciences, v. 31, p. 1309-1319.

_____ 1997a. The Romaine Formation in ARCO-NACP-LGCP wells (Anticosti Island), high-frequency cyclicity and significance for porosity. A Confidential Report to Shell Canada, 28p.

_____ 1997b. The Mingan and Romaine formations in LGPL-Oil River-Highcliff wells (Anticsoti Island): high-frequency cyclicity and significance for porosity. A confidential report to Shell Canada, 15p.

_____ 1998. Porosity log for the Romaine Formation in the LGCP and NACP wells. A confidential report to Shell Canada, 10p.

_____ 2004. Hydrothermal dolomite reservoirs in Ordovician and Silurian successions of eastern Quebec: A future success story. Canadian Society of Petroleum Geologists, Annual Meeting, Calgary, Abstract on CD-Rom.

_____ 2005a. Hydrothermal dolomitization in the Lower Silurian La Vieille Formation in northeastern New Brunswick: field evidence and implication for hydrocarbon exploration. Geological Survey of Canada, Current Research, paper 2005-D1, 10p.

_____ 2005b. Hydrothermal Dolomite Reservoirs in Eastern Canada—a Promising Newly Recognized Play in Paleozoic Carbonates. American Association of Petroleum Geologists / Canadian Society of Petroleum Geologists, Joint annual meeting, Calgary 2005, http://aapg.confex.com/aapg/cal2005/techprogram/A94054.htm.

_____ and Morin, C. 2004. Hydrothermal dolomitization in the Lower Silurian Sayabec Formation in northern Gaspé – Matapédia (Québec): Constraint on timing of porosity and regional significance for hydrocarbon reservoirs. Bulletin of Canadian Petroleum Geology, v. 52, p. 256-269.

Long, D.G.F. 1997. Seven millions years of storm redistribution along the east coast of Laurentia: Transport mechanisms, current systems and influence of siliciclastics on reef development in the Late Ordovician and Early Silurian carbonate ramp of Anticosti Island, Québec, Canada. Proceedings of the 8th International Coral Reef Symposium, v. 2, p. 1743-1748.

Loucks, R.G. 1999. Paleocave carbonate reservoirs: origin, burial-depth, spatial complexities, and reservoir implications. American Association of Petroleum Geologists Bulletin, v. 83, p. 1795-1834.

_____ 2003. Origin of Lower Ordovician Ellenburger Group brecciated and fractured reservoirs in west Texas: paleocave, thermobaric, tectonic or all of the above? Abstract, American Association of Petroleum Geologists, Annual Meeting, Program with abstracts.

_____ and Anderson, J. H. 1985. Depositional facies, diagenetic terranes, and porosity development in Lower Ordovician Ellenburger Dolomite, Puckett field, west Texas. In: Carbonate Petroleum Reservoirs, P.O. Roehl and P.W. Choquette (eds.). Springer-Verlag, New York, p. 19-38.

Lynch, G. and Grist, A.M. 2002. Thermal modelling of the Laurentian Margin beneath Anticosti Island using AFTA, 1D well profiles and bulk fluid inclusions. Canadian Society of Petroleum Geologists, Diamond Jubilee Convention, Calgary 2002. Program with abstracts, p. 210.

_____ and Trollope, S.W. 2001. Dolomitization, platform collapse, and reservoir development in Ordovician carbonates of Anticosti Island, Gulf of St. Lawrence. Canadian Society of Petroleum Geologists, Annual Meeting, "Rock the Foundation" Calgary 2001. Program with Abstracts, p. 126-1 to 126-6.

Machel, H.G. 1987. Saddle dolomite as a by-product of chemical compaction and thermochemical sulfate reduction. Geology, v. 15, p. 936-940.

_____ and Lonee, J. 2002. Hydrothermal dolomite – a product of poor definition and imagination. Sedimentary Geology, v. 152, p. 163-171.

Montañez, I.P. 1994. Late diagenetic dolomitization of Lower Ordovician Upper Knox carbonates: a record of the hydrodynamic evolution of the southern Appalachian Basin. American Association of Petroleum Geologists, Bulletin, v. 78, p. 1210-1239.

_____ and Read J.F. 1992. Eustatic control on early dolomitization of cyclic peritidal carbonates: evidence from the Early Ordovician Upper Knox Group, Appalachians. Geological Society of America Bulletin, v. 104, p. 872-886.

Ministère des Richesses naturelles du Québec (MRN). 1974. Data on wells drilled for petroleum and natural gas in the Gaspé and Gulf of St. Lawrence area (Anticosti and Magdelen Islsnd). Ministère des Richesses naturelles du Québec, Direction générale de l'Énergie. 202p.

Mussman, W.J. and Read, J.F. 1986, Sedimentology and development of a passive to covergent margin unconformity: Middle Ordovician Knox Unconformity, Virginia Appalachians, Geological Society of America Bulletin, v. 97, p. 282-295.

Oakey, G.N. and Dehler, S.A. 2004. Magnetic anomaly map, Gulf of St. Lawrence and surrounds, Atlantic Canada. Geological Survy of Canada, Open File 1815, 1:500 000.

Qing, H. and Veizer, J. 1994. Oxygen and carbon isotopic composition of Ordovician brachiopods: Implications for coeval seawater. Geochimica et Cosmochimica Acta, v. 58, p. 4429-4442.

Radke, B.M. and Mathis, R.L. 1980. On the formation and occurrence of saddle dolomite. Journal of Sedimentary Petrology, v. 50, p. 1149-1168.

Raymond, D.E. and Osborne, W.E. 1991. Stratigraphy and exploration of the Knox Group in the Appalachian fold and thrust belt and Black Warrior Basin of Alabama. In: Arbuckle Group core workshop and field trip, K.S. Johnson (ed.). Oklahoma Geological Survey Special Publication 91-3, p. 163-180.

Read, J.F. 1989. Controls on evolution of Cambrian-Ordovician passive margin, U.S. Appalachians. In: Controls on carbonate platform and basin development. P. Crevello, J.L. Wilson, J.F. Sarg and J.F. Read (eds.). SEPM Special Publication 44, p. 147-166.

Riva, J. 1969. Middle and Upper Ordovician graptolite faunas of St. Lawrence Lowlands of Quebec, and of Anticosti Island. In: North Atlantic - Geology and Continental Drift. M. Kay (ed.). American Association of Petroleum Geologists Bulletin, Memoir 12, p. 513-5

Roedder, E. 1984. Fluid inclusions. Reviews in Mineralogy, v. 12, 644p.

Roksandic, M.M. and Granger, B. 1981. Structural styles of Anticosti Island, Gaspé Passage, and eastern Gaspé Peninsula inferred from reflection seismic data. In: Subcommission of Silurian Stratigraphy, Ordovician-Silurian boundary working group. Field meeting, Anticosti-Gaspé, 1981, P.J. Lespérance (ed.). Vol. II Stratigraphy and paleontology, Université de Montréal, Montréal, Québec, p. 211-221.

Salad Hersi, O., Lavoie, D. and Nowlan, G.S. 2003. Reappraisal of the Beekmantown Group sedimentology and stratigraphy, Montréal area, southwestern Quebec: implications for understanding the depositional evolution of the Lower-Middle Ordovician Laurentian passive margin of eastern Canada. Canadian Journal of Earth Sciences, v. 40, p. 149-176.

Sami, T. and Desrochers, A. 1992. Episodic sedimentation on an early Silurian, storm-dominated carbonate ramp, Becsie and Merrimack formations, Anticosti Island, Canada. Sedimentology, v. 39, p. 355-381.

Sanford, B.V. 1993. St. Lawrence Platform – Geology; Chapter 11 In: Sedimentary Cover of the Craton in Canada, D.F. Stott and J.D. Aitken (eds.). Geological Survey of Canada, Geology of Canada, n. 5, p. 723-786.

Saunders, C., Strong, D.F. and Sangster, D.F. 1992. Carbonate-hosted lead-zinc deposits of western Newfoundland. Geological Survey of Canada Bulletin 419, 78p.

Smith, L.B. 2004. Fault-controlled hydrothermal alteration of carbonate reservoirs. Geological Association of Canada – Mineralogical Association of Canada Joint annual meeting, St. Catherines 2004. Abstract on CD-Rom.

_____, Palmer, A. and Davies, G.R. 2005. Tectono-thermobaric carbonate breccia reservoirs: A major remaining resource in North America. American Association of Petroleum Geologists / Canadian Society of Petroleum Geologists Joint Annual Meeting, Calgary 2005. Program with abstracts.

Snedecor,G. W. and Cochran,W. A. 1967. Statiscical Methods. Sixth edition, ninth printing, 1978. Iowa State University Press, Ames, Iowa, U.S.A., 593p.

Stasiuk, L.D. and Snowdon, L.R. 1997. Fluorescence micro-spectrometry of synthetic and natural hydrocarbon fluid inclusions: crude oil geochemistry, density and application to petroleum migration. Applied Geochemistry, v. 12, p. 229-241.

Stenzel, S.R., Knight, I. and James, N.P. 1990. Carbonate platform to foreland basin: revised stratigraphy of the Table Head Group (Middle Ordovician), western Newfoundland. Canadian Journal of Earth Sciences, v. 27, p. 14-26.

Van Staal, C.R., Dewey, J.F., Mac Niocaill, C. and McKerrow, W.S. 1998. The Cambrian-Silurian tectonic evolution of the northern Appalachians and British Caledonides: history of a complex, west and southwest Pacific-type segment of Iapetus. In: Lyell: the Past is the key to the Present. D.J. Blundell and A.C. Scott (eds.). Geological Society, London, Special Publication 143, p. 199-242.

Veizer, J. 1983. Trace elements and isotopes in sedimentary carbonates. Reviews in Mineralogy, v. 11, p. 265-299.

Manuscript received: May 9, 2005

Revised manuscript accepted: October 3, 2005